Electronic Supplementary Information

o-Carborane decorated diboron-embedded multi-resonance TADF compounds featuring narrowband emission

Nhi Ngoc Tuyet Nguyen,[a†] Rafi Muhammad Lutfi,[a†] Taehwan Lee,[a,b] Jaehoon Jung*[a] and Min Hyung Lee*[a]

[a] Department of Chemistry, University of Ulsan, Ulsan 44610, Republic of Korea

[b] Current address: Department of Chemistry, Graduate School of Science, Kyoto University, Sakyo-ku, Kyoto 606-8502, Japan

Experimental

General considerations

All operations were performed under an inert nitrogen atmosphere using standard Schlenk and glove box techniques. Anhydrous grade solvents (Aldrich) were dried over activated molecular sieves (5Å). Spectrophotometric-grade toluene and tetrahydrofuran (THF) were used as received from Aldrich and Alfa, respectively. Commercial reagents were used without further purification after purchase. *N*^{1},*N*^{3}-diphenylbenzene-1,3-diamine was synthesized according to the modified literature procedures.[1] Deuterated solvents from Eurisotop were used. NMR spectra were recorded on a Bruker AVANCE III HD 400 (400.13 MHz for ^{1}H, 100.61 MHz for ^{13}C, 128.38 MHz for ^{11}B) spectrometer at ambient temperature. Chemical shifts are given in ppm, and are referenced against external Me_4Si (^{1}H, ^{13}C) and $BF_3{\cdot}OEt_2$ (^{11}B). Mass spectra were obtained using a JEOL JMS700 high-resolution EI-mass spectrometer (HR EI-MS) at the Korea Basic Science Institute (KBSI), Daegu, Korea. Elemental analyses were performed on a Flash 2000 elemental analyzer (Thermo Scientific). Thermogravimetric analysis (TGA) was performed with a TA Instruments Q50 under an N_2 atmosphere at a heating rate of 10 °C/min. Cyclic voltammetry experiments were carried out using a CHI600E system.

Synthesis

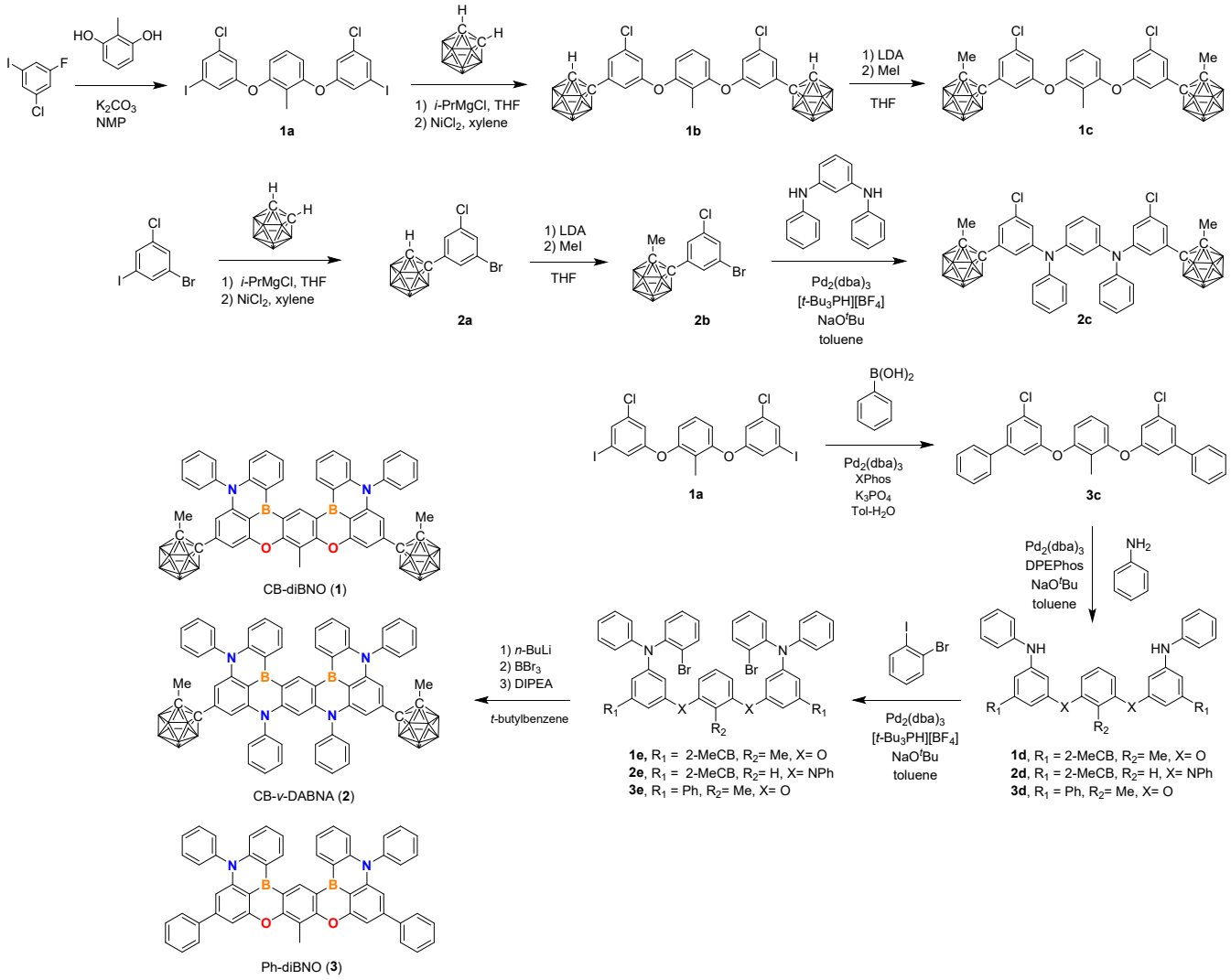

Scheme S1 Synthesis of CB-diBNO (**1**), CB-*v*-DABNA (**2**), and Ph-diBNO (**3**).

Synthesis of 1a

2-Methylresorcinol (0.36 g, 2.93 mmol) and K_2CO_3 (0.81 g, 5.85 mmol) were dissolved in *N*-methylpyrrolidone (NMP, 30 mL) at room temperature. After stirring for 30 min, 1-chloro-3-fluoro-5-iodobenzene (1.5 g, 5.85 mmol) was added to the solution. The mixture was stirred overnight at 170 °C. After cooling to room temperature, the reaction mixture was poured into a large amount of water. The product was extracted with ethyl acetate, and the combined organic layer was dried over anhydrous $MgSO_4$. After filtration and evaporation of the solvent, the crude product was purified by column chromatography on silica gel (eluent: dichloromethane/*n*-hexane = 1:4, v/v) to give **1a** as a white solid (Yield = 1.40 g, 81%). ^{1}H NMR ($CDCl_3$): δ 7.22 (dt, J = 3.9, 2.1 Hz, 3H), 6.99–6.96 (m, 2H), 6.86 (dd, J = 4.0, 1.9 Hz, 3H), 6.83 (s, 1H), 2.06 (s, 3H). ^{13}C NMR ($CDCl_3$): δ 158.90, 154.65, 136.08, 127.85, 125.90, 123.31, 118.88, 117.06, 116.51, 9.57.

Synthesis of 1b

To a THF solution (5 mL) of *o*-carborane (0.47 g, 3.3 mmol) was slowly added ^{i}PrMgCl (2.0 M in THF, 1.98 mL, 3.96 mmol) at 0 °C, and the mixture was stirred for 1 h. After replacement of THF with xylene (5 mL), **1a** (1.65 mmol) and $NiCl_2$ (8.6 mg, 0.07 mmol) were added, and the reaction mixture was heated at 140 °C for 12 h in a closed flask. After cooling down to room temperature, the reaction was quenched with water (10 mL) and the organic portion was extracted with diethyl ether (20 mL × 3). The combined organic layer was dried over anhydrous $MgSO_4$, filtered, and evaporated to dryness. The crude product was purified by column chromatography on silica gel (eluent: dichloromethane/*n*-hexane = 1:8, v/v) to give **1b** as a white solid (Yield = 0.54 g, 52%). ^{1}H NMR ($CDCl_3$): δ 7.24 (s, 1H), 7.15 (t, J = 1.7 Hz, 2H), 7.05 (t, J = 2.0 Hz, 2H), 6.83 (dd, J = 7.4, 5.2 Hz, 4H), 3.94 (s, 2H), 2.06 (s, 3H). ^{13}C NMR ($CDCl_3$): δ 158.46, 154.54, 136.72, 136.04, 128.05, 123.15, 122.03, 118.32, 116.86, 115.67, 74.66, 59.97, 9.60.

Synthesis of 1c

Compound **1b** (0.50 g, 0.75 mmol) was dissolved in dry THF (20 mL) and lithium diisopropylamide (LDA, 1.13 mL, 2.25 mmol) was slowly added dropwise to the solution at −20 °C. After 1 h, an excess MeI (3.16 mmol) was added to the reaction mixture at −20 °C, and the mixture was stirred overnight at room temperature. The reaction was quenched by the addition of saturated aqueous NH_4Cl solution and extracted with diethyl ether (30 mL × 3). The organic portion was washed with water, dried over $MgSO_4$, filtered, and evaporated to dryness. The crude product was purified by column chromatography on silica gel (eluent: dichloromethane/*n*-hexane = 1:10, v/v) to give **1c** as a white solid (Yield = 0.30 g, 63%). ^{1}H NMR ($CDCl_3$): δ 7.35 (s, 2H), 7.21–7.18 (m, 2H), 6.94 (t, J = 1.8 Hz, 2H), 6.84 (s, 2H), 6.82 (s, 1H), 2.08 (s, 3H), 1.77 (s, 6H). ^{13}C NMR ($CDCl_3$): δ 158.40, 154.70, 136.03, 134.22, 129.77, 128.04, 125.55, 123.05, 119.49, 119.46, 119.18, 118.92, 116.75, 80.15, 23.41, 9.61.

Synthesis of 2a

This compound was prepared in a manner analogous to the synthesis of **1b** using 1-bromo-3-chloro-5-iodobenzene (0.7 g, 2.21 mmol), affording the title compound as a white solid (Yield: 0.56 g, 72%). ^{1}H NMR ($CDCl_3$): δ 7.74 (t, J = 1.5 Hz, 1H), 7.68–7.65 (m, 1H), 7.43 (t, J = 1.8 Hz, 1H), 3.93 (s, 1H). ^{13}C NMR ($CDCl_3$): δ 143.27, 140.94, 134.98, 134.70, 131.10, 76.41, 59.79.

Synthesis of 2b

This compound was prepared in a manner analogous to the synthesis of **1c** using **2a** (0.56 g, 1.67 mmol), affording the title compound as a white solid (Yield: 0.43 g, 74%). ^{1}H NMR ($CDCl_3$): δ 7.85 (s, 1H), 7.73 (d, J = 1.6 Hz, 2H), 1.72 (s, 6H). ^{13}C NMR ($CDCl_3$): δ 139.00, 137.38, 135.92, 133.47, 130.55, 82.80,

23.84.

Synthesis of 2c

A mixture of **2b** (0.43 g, 1.23 mmol), N^1,N^3-diphenylbenzene-1,3-diamine (0.50 g, 1.92 mmol), $Pd_2(dba)_3$ (52.7 mg, 0.058 mmol), [^{t}Bu$_3$PH][BF_4] (33.5 mg, 0.12 mmol), and NaO^{t}Bu (0.55 g, 5.76 mmol) in dry toluene (20 mL) were stirred overnight at 80 °C. After cooling down to room temperature, the mixture was filtered through a Celite pad, and washed with dichloromethane. After concentration of the filtrate under reduced pressure, the crude product was purified by column chromatography on silica gel using dichloromethane/*n*-hexane (1:5, v/v) as eluent to give **2c** as a white solid (Yield: 0.50 g, 81%). ^{1}H NMR ($CDCl_3$): δ 7.33 (t, J = 7.8 Hz, 6H), 7.08 (d, J = 7.5 Hz, 4H), 7.02 (d, J = 2.9 Hz, 2H), 6.88 – 6.81 (m, 6H), 6.73 (d, J = 10.5 Hz, 2H), 1.67 (s, 6H). ^{13}C NMR ($CDCl_3$): δ 164.31, 161.86, 149.49, 147.73, 145.93, 133.30, 131.10, 129.95, 125.50, 125.25, 121.80, 121.44, 119.99, 111.21, 110.97, 110.14, 109.90, 80.85, 77.25, 23.27.

Synthesis of 3c

A mixture of **1a** (0.4 g, 0.67 mmol), phenylboronic acid (22 mg, 0.179 mmol), $Pd_2(dba)_3$ (30.7 mg, 0.03 mmol), XPhos (32 mg, 0.07 mmol), and K_3PO_4 (0.23 g, 1.67 mmol) was dissolved in degassed toluene (10 mL)/water (1 mL) solvent. The solution was refluxed for 14 h under nitrogen atmosphere. After cooling to room temperature, the reaction mixture was poured into a large amount of water. The product was extracted with ethyl acetate, and the organic portion was dried over anhydrous $MgSO_4$, filtered, and evaporated to dryness. The crude product was purified by column chromatography on silica gel (eluent: dichloromethane/*n*-hexane = 1:6, v/v) to give **3c** as a white solid (Yield = 0.23 g, 69%). ^{1}H NMR ($CDCl_3$): δ 7.54 (d, J = 7.3 Hz, 4H), 7.41 (dt, J = 23.0, 6.9 Hz, 6H), 7.30 (s, 2H), 7.21 (t, J = 8.1 Hz, 1H), 7.09 (s, 2H), 6.92–6.83 (m, 4H), 2.18 (s, 3H). ^{13}C NMR ($CDCl_3$): δ 158.80, 155.33, 144.40, 139.44, 135.57, 129.07, 128.32, 127.54, 127.22, 123.00, 121.87, 116.31, 114.62, 9.65.

Synthesis of 1d

A mixture of **1c** (0.3 g, 0.45 mmol), aniline (0.13 g, 1.35 mmol), $Pd_2(dba)_3$ (13.4 mg, 0.01 mmol), DPEPhos (14.5 mg, 0.03 mmol), and NaO^{t}Bu (0.13 g, 1.35 mmol) in dry toluene (20 mL) was stirred overnight at 90 °C. After cooling down to room temperature, the mixture was filtered through a Celite pad, washed with dichloromethane, and the filtrate was concentrated under reduced pressure. The crude product was purified by column chromatography on silica gel using dichloromethane/*n*-hexane (1:3, v/v) as eluent to give **1d** as a white solid (Yield: 0.65 g, 69%). ^{1}H NMR ($CDCl_3$): δ 7.31 (dd, J = 8.3, 7.5 Hz, 4H), 7.17 (t, J = 8.2 Hz, 1H), 7.10–6.98 (m, 8H), 6.76 (d, J = 8.1 Hz, 4H), 6.62 (s, 2H), 5.81 (s, 2H), 2.12

(s, 3H), 1.79 (s, 6H). ^{13}C NMR ($CDCl_3$): δ 158.75, 155.24, 145.39, 141.15, 133.40, 129.65, 127.22, 122.79, 122.37, 119.28, 115.48, 113.72, 112.14, 106.75, 81.62, 23.25, 9.47.

Synthesis of 2d

This compound was prepared in a manner analogous to the synthesis of **1d** using **2c** (0.50 g, 0.63 mmol), affording the title compound as a white solid (Yield: 0.45 g, 82%). ^{1}H NMR ($CDCl_3$): δ 7.33 (t, J = 7.8 Hz, 6H), 7.24 (d, J = 8.1 Hz, 2H), 7.17 – 7.11 (m, 8H), 7.07 (d, J = 7.6 Hz, 6H), 7.01 (d, J = 1.6 Hz, 4H), 6.86 – 6.79 (m, 4H), 5.81 (s, 2H), 1.67 (s, 6H). ^{13}C NMR ($CDCl_3$): δ 157.73, 156.66, 149.44, 148.44, 147.13, 140.72, 139.01, 138.87, 132.63, 130.09, 129.71, 125.43, 122.73, 121.48, 119.93, 118.59, 113.62, 111.58, 81.56, 77.37, 23.35.

Synthesis of 3d

This compound was prepared in a manner analogous to the synthesis of **1d** using **3c** (0.23 g, 0.46 mmol), affording the title compound as a white solid (Yield: 0.20 g, 71%). ^{1}H NMR ($CDCl_3$): δ 7.52 (d, J = 7.3 Hz, 4H), 7.39 (t, J = 7.4 Hz, 4H), 7.35 (s, 1H), 7.33–7.30 (m, 2H), 7.27 (d, J = 7.7 Hz, 4H), 7.13 (d, J = 7.6 Hz, 4H), 7.00 (s, 2H), 6.96 (t, J = 7.3 Hz, 2H), 6.84 (d, J = 8.2 Hz, 2H), 6.73 (s, 2H), 6.63 (t, J = 2.0 Hz, 2H), 5.81 (s, 2H), 2.23 (s, 3H). ^{13}C NMR ($CDCl_3$): δ 159.38, 155.93, 145.34, 144.08, 142.60, 140.96, 129.67, 127.87, 127.32, 127.11, 122.69, 121.90, 118.89, 115.55, 110.53, 109.00, 105.42, 9.76.

Synthesis of 1e

This compound was prepared in a manner analogous to the synthesis of **2c** using **1d** (0.65 g, 0.84 mmol) and 1-bromo-2-iodobenzene (0.55 g, 1.95 mmol), affording the title compound as a white solid (Yield: 0.69 g, 76%). ^{1}H NMR ($CDCl_3$): δ 7.66 (dd, J = 8.0, 1.3 Hz, 2H), 7.35 (dd, J = 7.6, 1.2 Hz, 2H), 7.29 (d, J = 7.9 Hz, 3H), 7.24 (dd, J = 7.9, 1.6 Hz, 2H), 7.18 (dd, J = 7.7, 1.3 Hz, 2H), 7.09–7.01 (m, 8H), 6.79 (d, J = 1.7 Hz, 2H), 6.73 (d, J = 1.8 Hz, 2H), 6.61–6.55 (m, 4H), 2.09 (s, 3H), 1.72 (s, 6H). ^{13}C NMR ($CDCl_3$): δ 158.03, 155.67, 148.67, 145.61, 144.37, 134.79, 132.98, 131.59, 129.72, 129.57, 129.41, 128.38, 126.86, 125.22, 124.12, 123.54, 117.59, 113.81, 113.40, 111.56, 81.62, 77.32, 23.31, 9.46. ^{11}B NMR ($CDCl_3$): δ −4.65 (4B), −10.19 (16B). HRMS (FAB): m/z [M]+ Calcd for $C_{49}H_{56}Br_2N_2O_2B_{20}$: 1082.4570; Found: 1082.4574.

Synthesis of 2e

This compound was prepared in a manner analogous to the synthesis of **2c** using **2d** (0.45 g, 0.49 mmol) and 1-bromo-2-iodobenzene (0.42 g, 1.47 mmol), affording the title compound as a white solid (Yield: 0.45 g, 75%). ^{1}H NMR ($CDCl_3$): δ 7.61–7.58 (m, 2H), 7.30 (d, J = 7.6 Hz, 2H), 7.19 (t, J = 7.8 Hz, 10H),

7.11 (t, J = 8.3 Hz, 4H), 7.00 (d, J = 7.2 Hz, 4H), 6.95 (dd, J = 7.6, 3.6 Hz, 10H), 6.76 (s, 2H), 6.75 (s, 1H), 6.70 (dd, J = 8.0, 2.1 Hz, 2H), 6.62 (d, J = 9.9 Hz, 4H), 1.60 (s, 6H). ^{13}C NMR ($CDCl_3$): δ 158.04, 155.67, 148.68, 145.62, 134.79, 132.98, 131.59, 129.72, 129.57, 129.41, 128.39, 126.87, 125.22, 124.12, 123.54, 123.52, 117.60, 113.41, 81.61, 77.32, 23.30. ^{11}B NMR ($CDCl_3$): δ −4.22 (4B), −10.79 (16B). HRMS (FAB): m/z [M]+ Calcd for $C_{60}H_{64}Br_2N_4B_{20}$: 1218.5360; Found: 1218.5361.

Synthesis of 3e

This compound was prepared in a manner analogous to the synthesis of **2c** using **3d** (0.20 g, 0.33 mmol) and 1-bromo-2-iodobenzene (0.28 g, 0.99 mmol), affording the title compound as a white solid (Yield: 0.20 g, 67%). ^{1}H NMR ($CDCl_3$): δ 7.64 (d, J = 8.1 Hz, 2H), 7.41 (d, J = 7.2 Hz, 4H), 7.36–7.27 (m, 12H), 7.24 (d, J = 8.0 Hz, 3H), 7.14–7.05 (m, 7H), 7.04–6.97 (m, 3H), 6.89 (s, 2H), 6.70 (d, J = 7.9 Hz, 4H), 6.57 (s, 2H), 2.17 (s, 3H). ^{13}C NMR ($CDCl_3$): δ 158.54, 156.08, 148.85, 146.59, 145.23, 143.45, 140.74, 134.71, 131.76, 129.61, 129.30, 129.06, 128.89, 128.78, 127.75, 127.68, 127.22, 123.89, 122.89, 116.19, 115.97, 115.73, 114.84, 114.58, 114.04, 110.38, 110.13, 9.56. HRMS (FAB): m/z [M]+ Calcd for $C_{55}H_{40}Br_2N_2O_2$: 918.1457; Found: 918.1453.

Synthesis of 1

To a solution of **1e** (0.69 g, 0.64 mmol) in *t*-butylbenzene (20 mL) was added dropwise *n*-BuLi (2.5 M in hexane, 0.56 mL, 1.41 mmol) at −30 °C. After stirring at 60 °C for 2 h, hexane was removed in *vacuo.* Boron tribromide (0.18 mL, 1.92 mmol) was added slowly at −30 °C, and the mixture was stirred at 50 °C for 2 h. *N*,*N*-Diisopropylethylamine (DIPEA, 0.33 mL, 1.92 mmol) was added at 0 °C, and the reaction mixture was stirred at 160 °C for 12 h. After cooling down to room temperature, an aqueous solution of NaOAc was added, and the mixture was extracted with ethyl acetate (3 × 30 mL). The combined organic layer was dried over $MgSO_4$, filtered, and washed several times with ethyl acetate. The solution was concentrated under reduced pressure and filtered through a silica gel (eluent: dichloromethane/*n*-hexane = 1:5) to give a yellow solid. The product was further purified by crystallization, affording the title compound as a bright yellow solid (Yield: 0.15 g, 26%). ^{1}H NMR ($C_2D_2Cl_4$): δ 10.13 (s, 1H), 9.15 (s, 2H), 7.82 (s, 4H), 7.68 (d, J = 67.1 Hz, 4H), 7.44 (d, J = 10.7 Hz, 8H), 6.98 (s, 2H), 6.66 (s, 2H), 2.87 (s, 3H), 1.72 (s, 6H). ^{13}C NMR ($C_2D_2Cl_4$): δ 159.27, 156.97, 149.91, 146.84, 145.51, 136.11, 134.07, 132.93, 130.93, 129.83, 128.28, 125.38, 124.77, 122.27, 118.89, 115.08, 114.77, 113.01, 83.10, 78.92, 24.64, 10.90. ^{11}B NMR ($C_2D_2Cl_4$): δ 42.4 (1B), −4.93 (4B), −9.99 (16B). Anal. Calcd (%) for $C_{49}H_{52}B_{22}N_2O_2$: C, 62.69; H, 5.58; N, 2.98. Found: C, 62.62; H, 5.57; N, 2.97. T_{d5} = 500 °C.

Synthesis of 2

This compound was prepared in a manner analogous to the synthesis of **1** using **2e** (0.45 g, 0.37 mmol), affording the title compound as a bright yellow solid (Yield: 0.08 g, 21%). ^{1}H NMR ($C_2D_2Cl_4$): δ 10.19 (s, 1H), 9.21 (d, J = 7.4 Hz, 2H), 7.77 (t, J = 7.2 Hz, 4H), 7.68 (d, J = 7.5 Hz, 3H), 7.55 (d, J = 8.8 Hz, 14H), 7.47 (s, 6H), 6.91 (d, J = 8.6 Hz, 2H), 6.61 (s, 2H), 1.70 (s, 6H). ^{13}C NMR ($C_2D_2Cl_4$): δ 161.15, 158.73, 151.69, 147.06, 145.79, 145.28, 141.75, 141.15, 135.80, 135.15, 131.16, 130.82, 129.59, 127.59, 127.26, 125.88, 121.30, 119.55, 119.11, 116.89, 112.05, 109.69, 105.52, 83.01, 78.48, 10.90. ^{11}B NMR ($C_2D_2Cl_4$): δ 41.0 (1B), −4.54 (4B), −9.90 (16B). Anal. Calcd (%) for $C_{60}H_{60}B_{22}N_4$: C, 67.04; H, 5.63; N, 5.21. Found: C, 66.83; H, 5.56; N, 5.20. T_{d5} = 489 °C.

Synthesis of 3

This compound was prepared in a manner analogous to the synthesis of **1** using **2e** (0.20 g, 0.22 mmol), affording the title compound as a bright yellow solid (Yield: 0.04 g, 24%). ^{1}H NMR (CD_2Cl_2): δ 10.22 (s, 1H), 9.26–9.22 (m, 2H), 7.80–7.75 (m, 4H), 7.71–7.68 (m, 2H), 7.57 (dd, J = 10.4, 3.4 Hz, 6H), 7.52–7.40 (m, 14H), 7.37 (dd, J = 8.5, 6.1 Hz, 2H), 6.91 (d, J = 8.7 Hz, 2H), 6.62 (d, J = 1.4 Hz, 2H), 2.93 (s, 3H). ^{13}C NMR (CD_2Cl_2): δ 155.30, 148.09, 147.12, 141.21, 135.50, 133.43, 133.07, 124.09, 123.24, 121.91, 121.18, 106.27, 82.81, 77.94, 35.58, 31.60, 23.50. ^{11}B NMR (CD_2Cl_2): δ 40.5 (1B). Anal. Calcd (%) for $C_{55}H_{36}B_2N_2O_2$: C, 84.85; H, 4.66; N, 3.60. Found: C, 84.87; H, 4.69; N, 3.62. T_{d5} = 519 °C.

Cyclic voltammetry

Cyclic voltammetry measurements were carried out with a three-electrode cell configuration consisting of platinum working and counter electrodes and a $Ag/AgNO_3$ (0.01 M in CH_3CN) reference electrode at room temperature. Tetra-*n*-butylammonium hexafluorophosphate (0.1 M) was used as the supporting electrolyte. The redox potentials were recorded at a scan rate of 100 mV/s and are reported with reference to the ferrocene/ferrocenium (Fc/Fc^+) redox couple. The HOMO energy levels were determined from the onset electrochemical oxidation (E_{onset}) of cyclic voltammograms while the LUMO energy levels were estimated from the optical bandgap (E_g) and the HOMO levels.

Photophysical measurements

UV/Vis absorption and photoluminescence (PL) spectra were recorded on a UV-2600 (Shimadzu) and an Edinburgh Instruments FLS1000 spectrophotometer, respectively. Photoluminescence quantum yields (PLQYs) all the samples were measured on an absolute PL quantum yield spectrophotometer (Quantaurus-QY C11347-11, Hamamatsu Photonics) equipped with a 3.3-inch integrating sphere. Transient PL decays were measured on an FLS1000 spectrophotometer with an excitation light source of EPL-375 laser for prompt fluorescence and VPL-375 laser for delayed fluorescence. The photophysical

analysis done by using FLS1000 and Quantaurus-QY C11347-11 spectrophotometers was conducted at total-period analysis center for Ulsan chemical industry of KBSI.

Theoretical calculations

Density functional theory (DFT) and time-dependent DFT (TDDFT) calculations were performed to investigate the ground and excited states of compounds **1**, **2**, and **3**. The Tamm-Dancoff approximation (TDA) was employed for TDDFT calculations.[2] The ground (S_0) states of compounds were optimized using DFT calculations, and their lowest singlet (S_1) and two triplets (T_1 and T_2) excited states were optimized using TDDFT calculations utilizing the PBE0 hybrid functional[3] and the def2-SVP[4] basis set implemented in GAUSSIAN 16 software package.[5] The influence of a solvent medium (toluene, ε = 2.3741) on the geometric and electronic structures was examined using the polarizable continuum model (PCM) model within a self-consistent reaction field (SCRF) approximation.[6] Additionally, a more polar solvent (THF, ε = 7.4257) was considered to investigate spectral quenching and bandwidth variation due to solvent medium. Natural transition orbital (NTO)[7] analysis was conducted to characterize the excited states, i.e., charge transfer (CT) and local excited states (LE), using the Multiwfn program.[8] The compositions of frontier molecular orbitals (FMOs) were investigated using the AOMix program.[9] The spin-orbit coupling matrix elements (SOCME) values were computed using the quasi-degenerate perturbation theory,[10] implemented in the ORCA software package,[11] and the same functional and basis set as used in the DFT and TDDFT calculations.

Root-mean-square-displacements (RMSDs) of the optimized structures at S_0 and S_1 states were analyzed using VMD software.[12] Additionally, electron-vibration coupling and Franck-Condon spectral analysis were performed through a sum-over-states approach[13] as implemented in the Molecular Materials Property Prediction Package (MOMAP 2020B).[14] The parameters for the simulation of PL spectra are provided in **Table S8**. The reorganization energy (λ_{ROE}^{k}) of vibrational mode, *k*, elucidated based on harmonic oscillator approximation, has a relation with its dimensionless Huang-Rhys factor (HR_k) as follows:

$$\lambda_{ROE}^{k} = HR_k \hbar \omega_k$$

$$HR_k = \frac{\omega_k D_k^2}{2\hbar}$$

where ω_k is the vibration frequency, and D_k denotes the normal coordinate displacement of mode *k*. The Huang-Rhys factor (HR^k) indicates the strength of electron-phonon coupling.

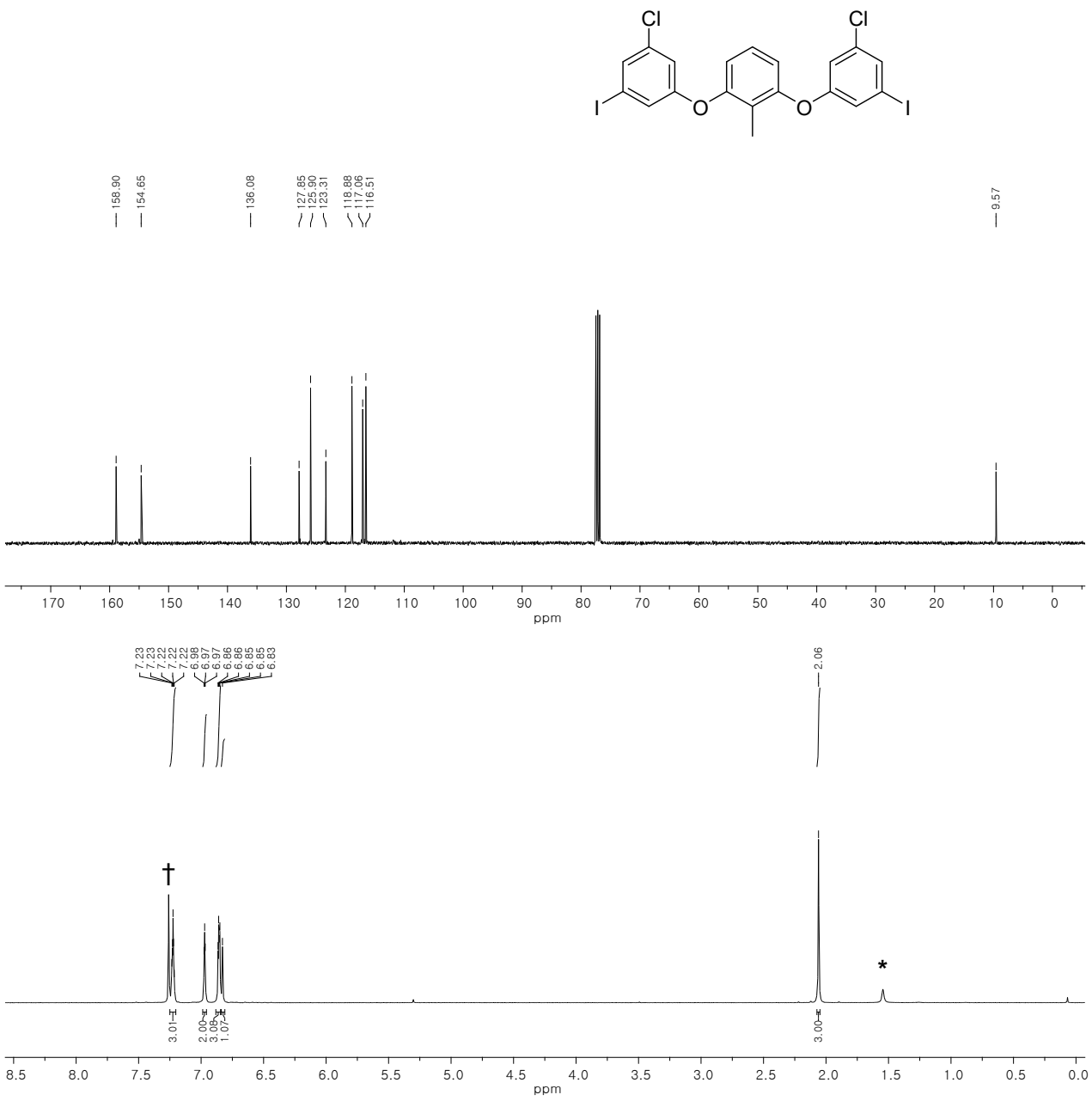

Fig. S1 ^{13}C (top) and ^{1}H (bottom) NMR spectra of **1a** (∗ and † from residual solvents).

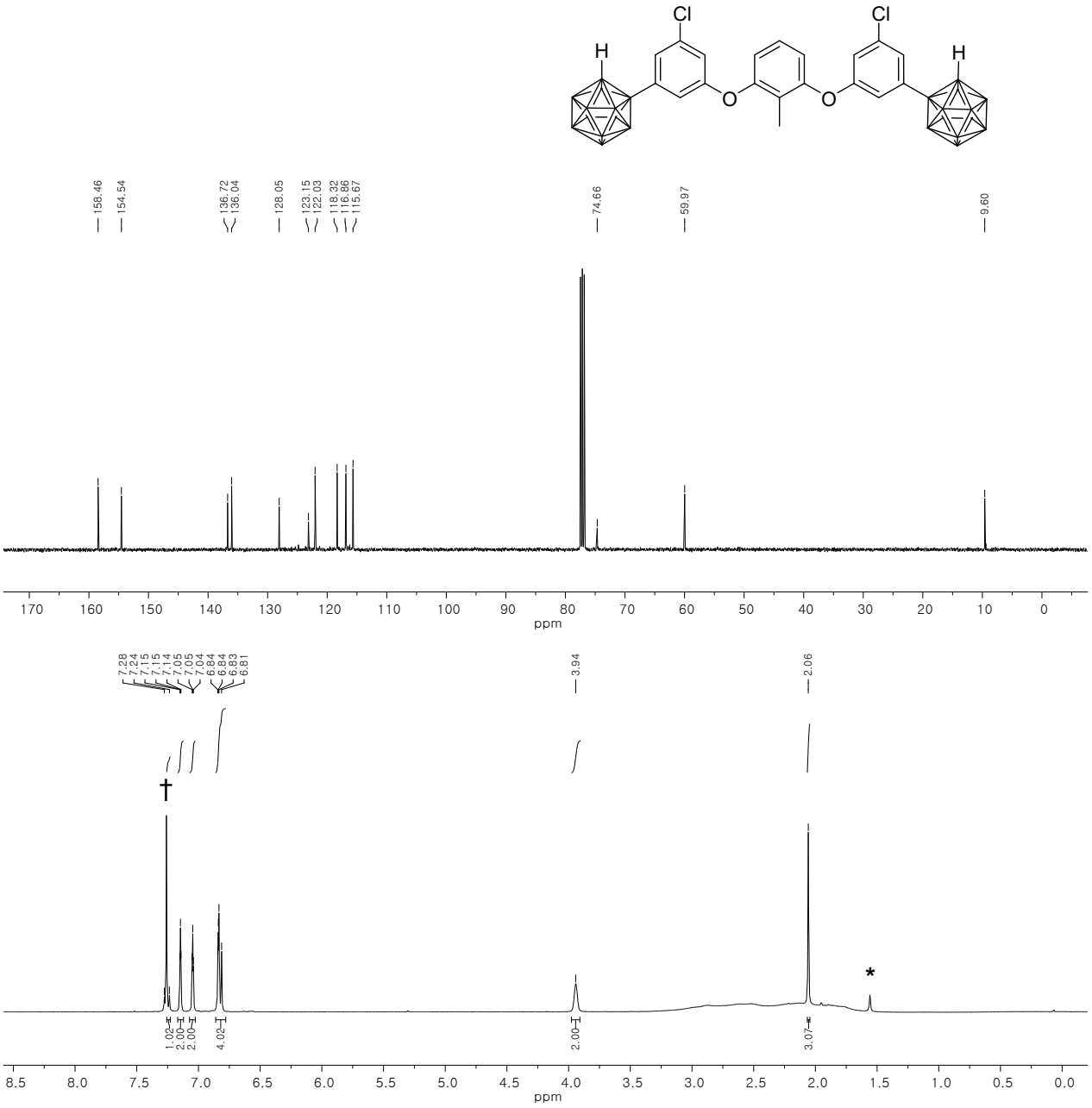

Fig. S2 ^{13}C (top) and ^{1}H (bottom) NMR spectra of **1b** (∗ and † from residual solvents).

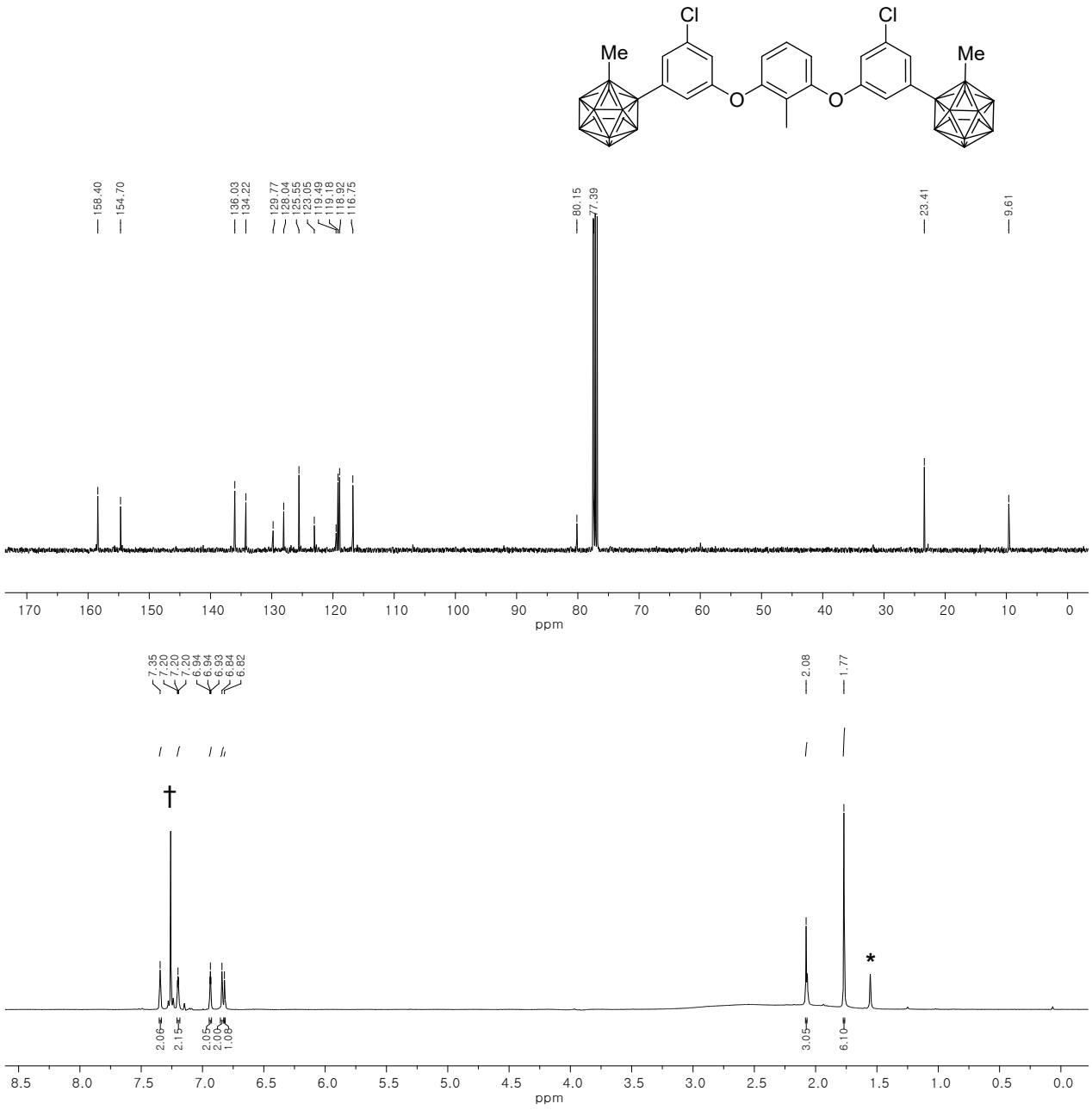

Fig. S3 ^{13}C (top) and ^{1}H (bottom) NMR spectra of **1c** (∗ and † from residual solvents).

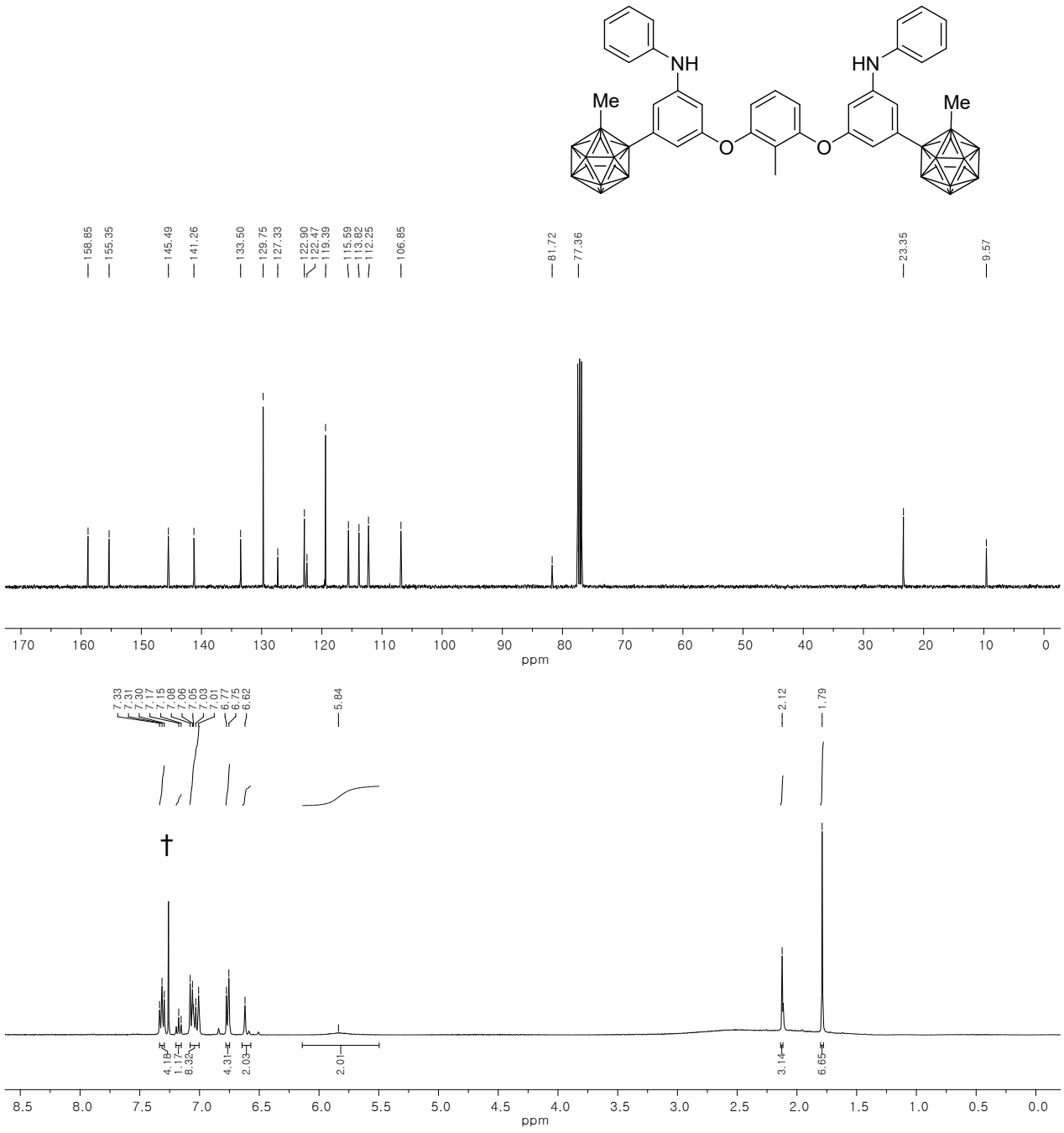

Fig. S4 ^{13}C (top) and ^{1}H (bottom) NMR spectra of **1d** (∗ and † from residual solvents).

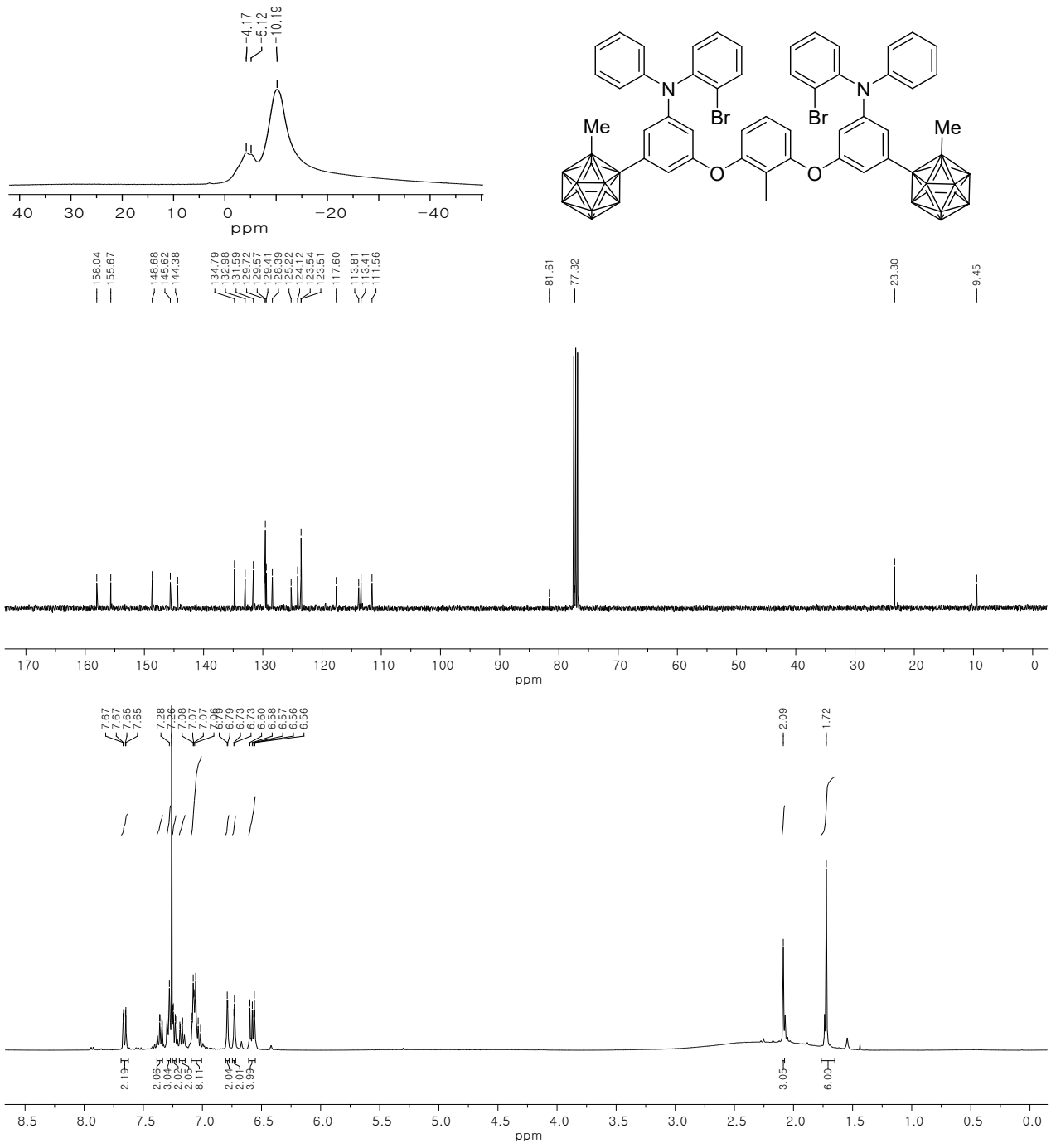

Fig. S5 ^{11}B (top), ^{13}C (middle), and ^{1}H (bottom) NMR spectra of **1e** (∗ and † from residual solvents).

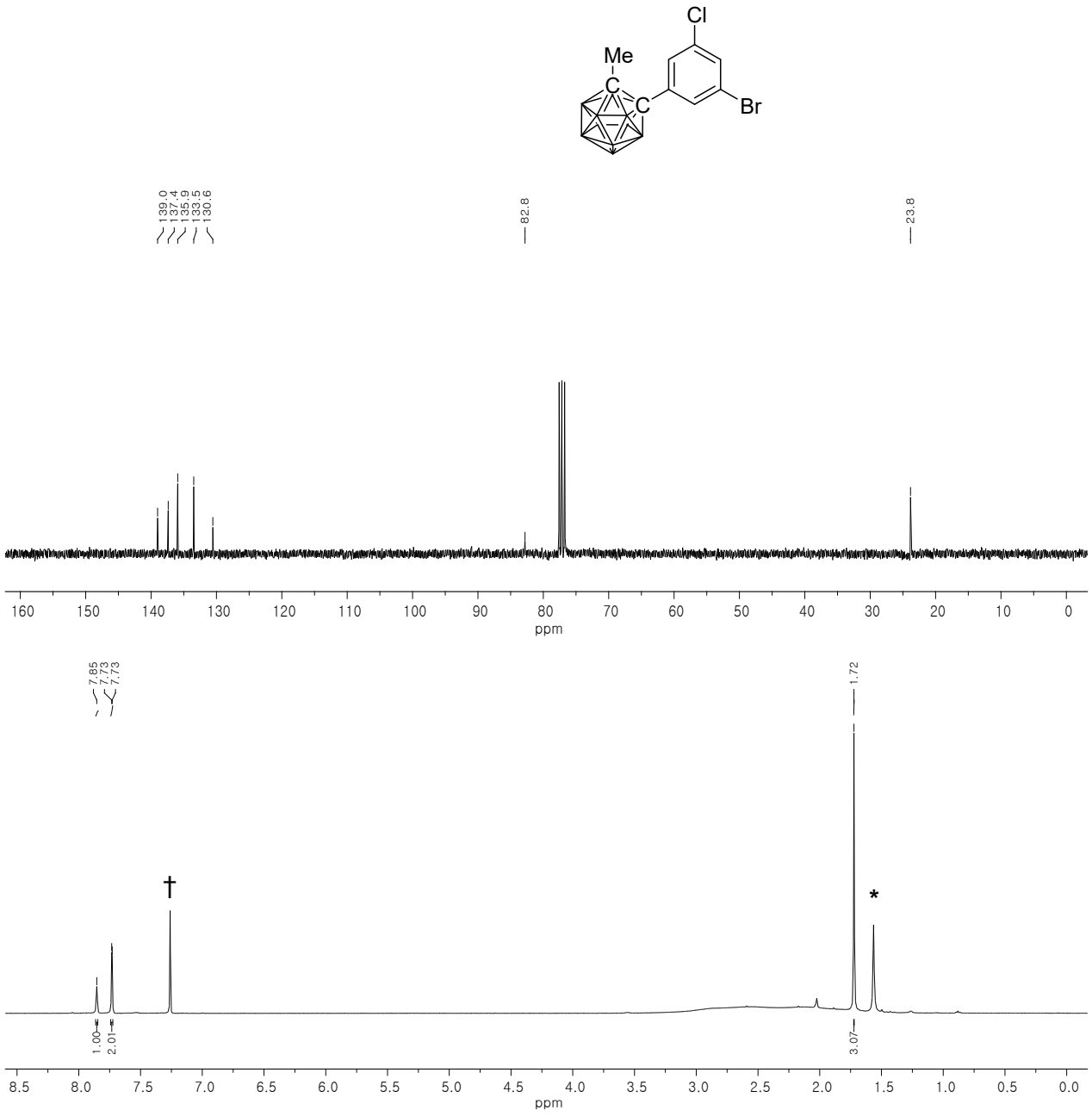

Fig. S6 ^{13}C (top) and ^{1}H (bottom) NMR spectra of **2b** (∗ and † from residual solvents).

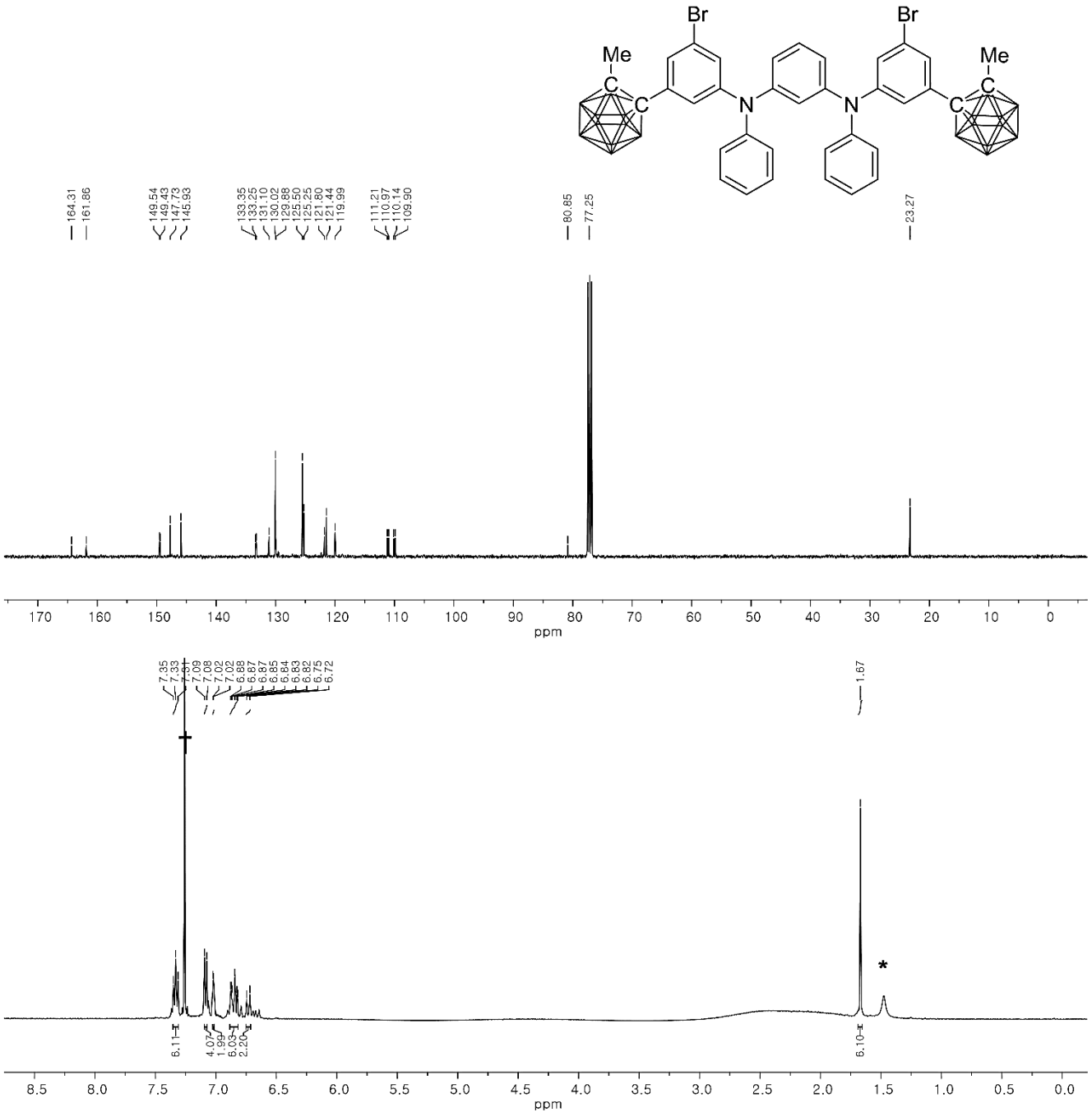

Fig. S7 ^{13}C (top) and ^{1}H (bottom) NMR spectra of **2c** (∗ and † from residual solvents).

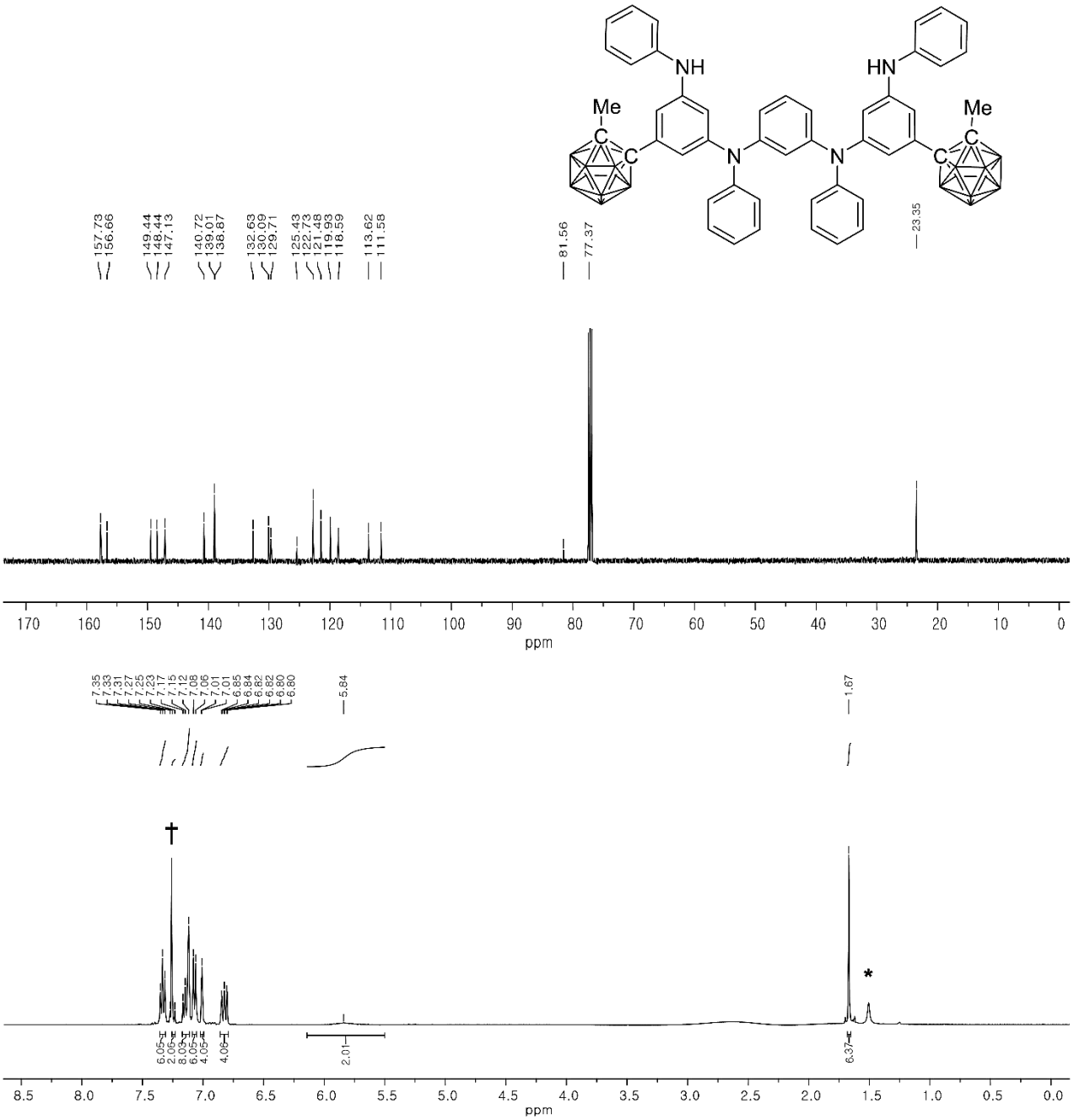

Fig. S8 ^{13}C (top) and ^{1}H (bottom) NMR spectra of **2d** (∗ and † from residual solvents).

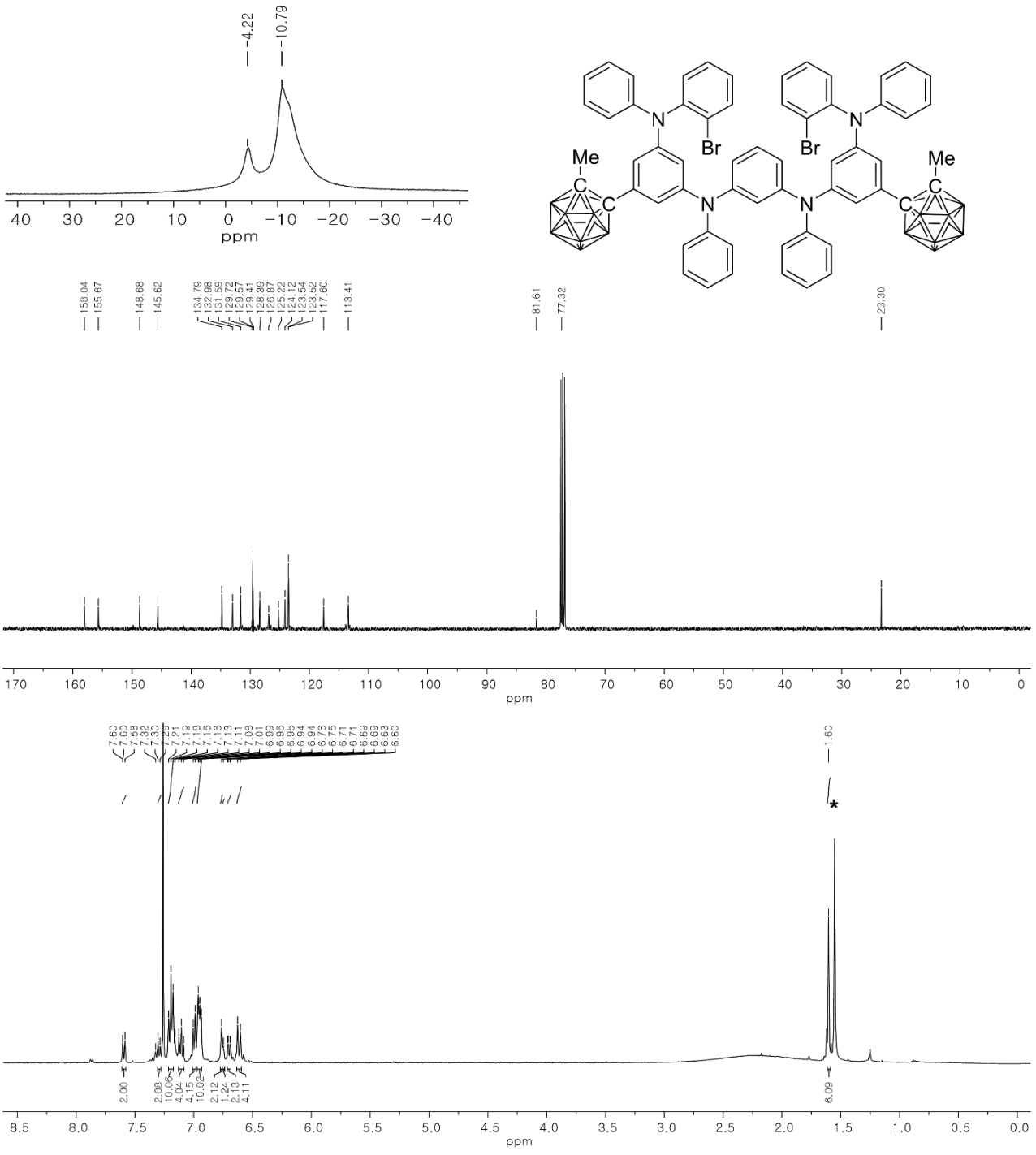

Fig. S9 ^{11}B (top), ^{13}C (middle), and ^{1}H (bottom) NMR spectra of **2e** (∗ and † from residual solvents).

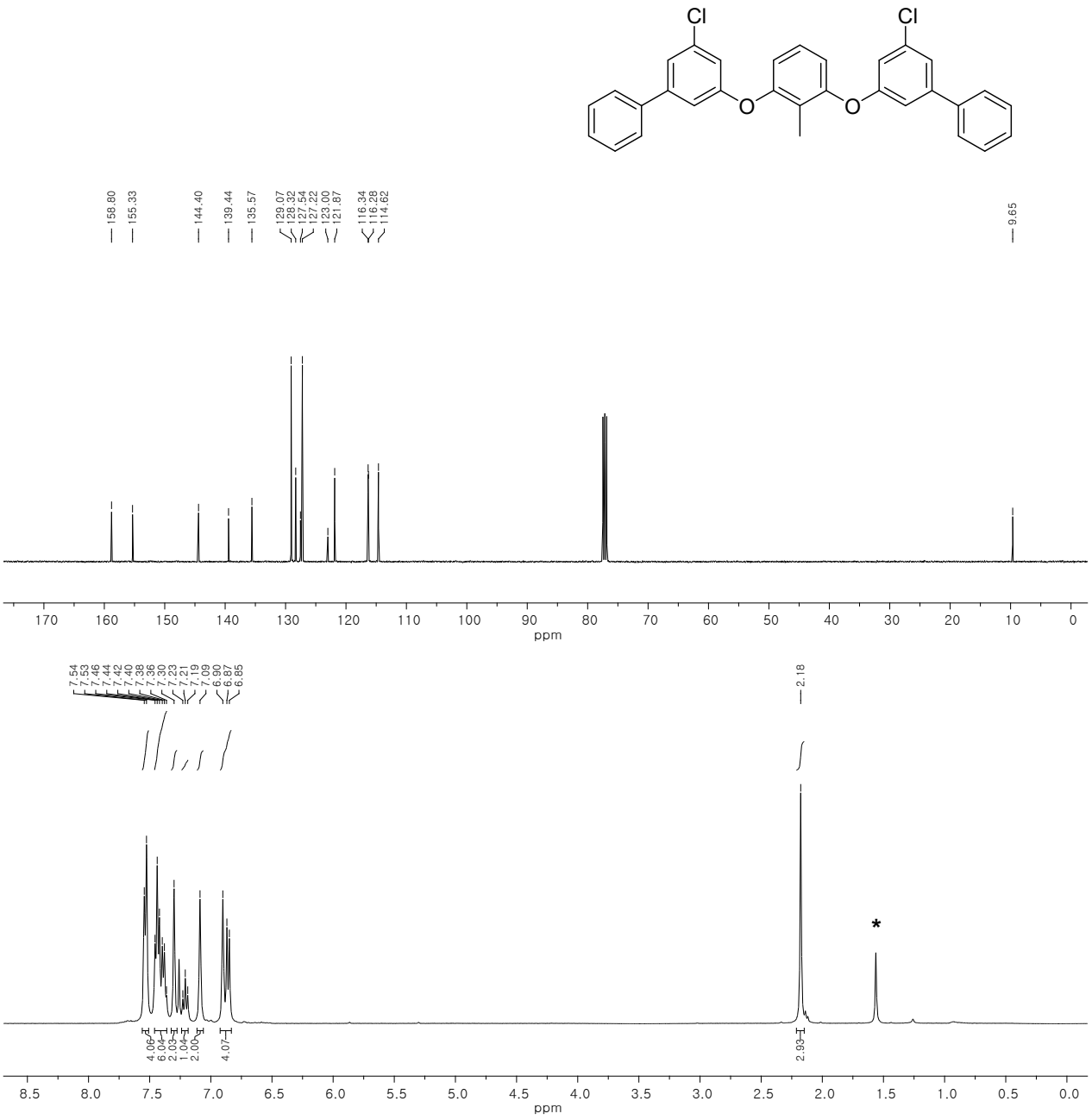

Fig. S10 ^{13}C (top) and ^{1}H (bottom) NMR spectra of **3c** (∗ and † from residual solvents).

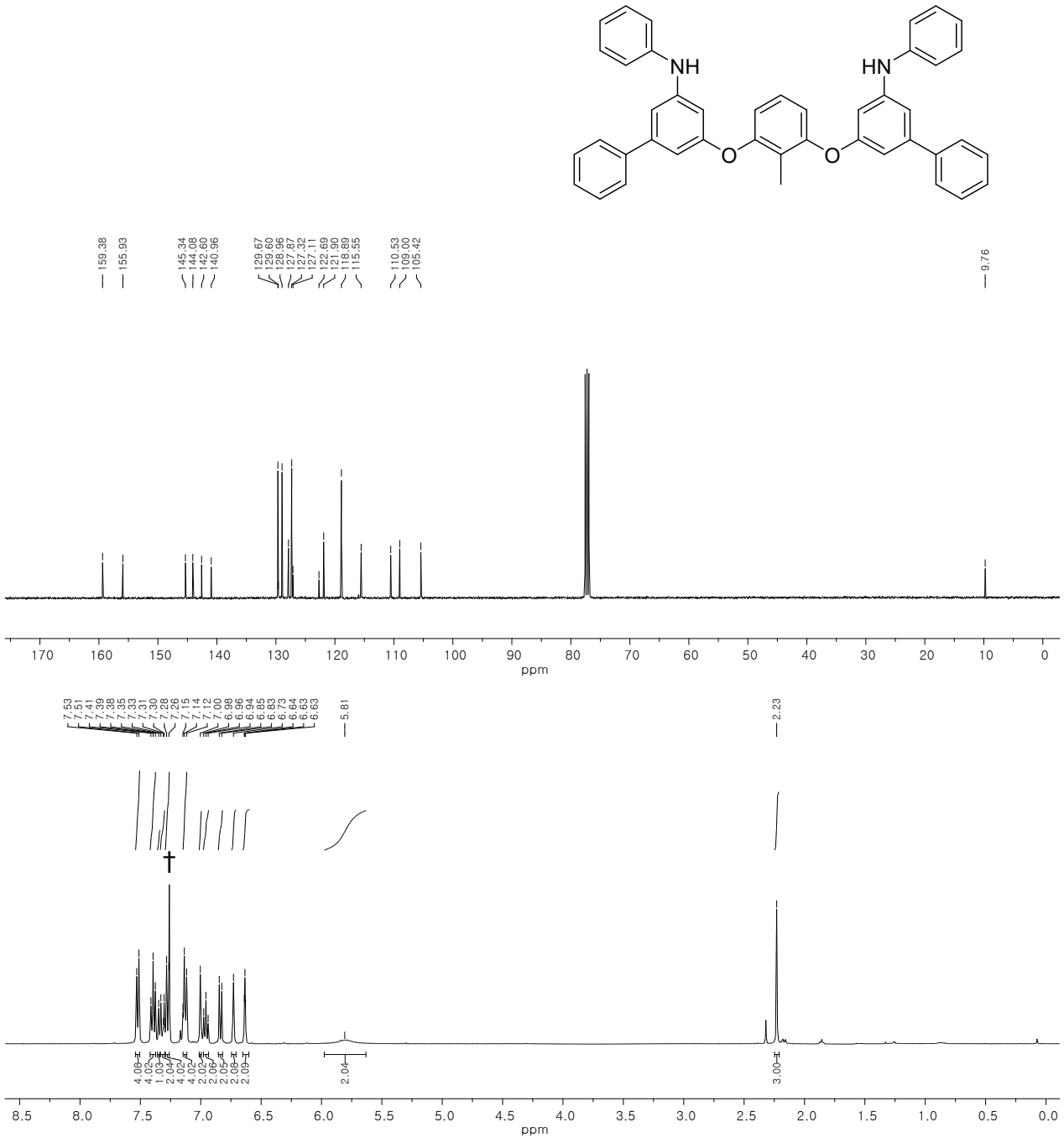

Fig. S11 ^{13}C (top) and ^{1}H (bottom) NMR spectra of **3d** (∗ and † from residual solvents).

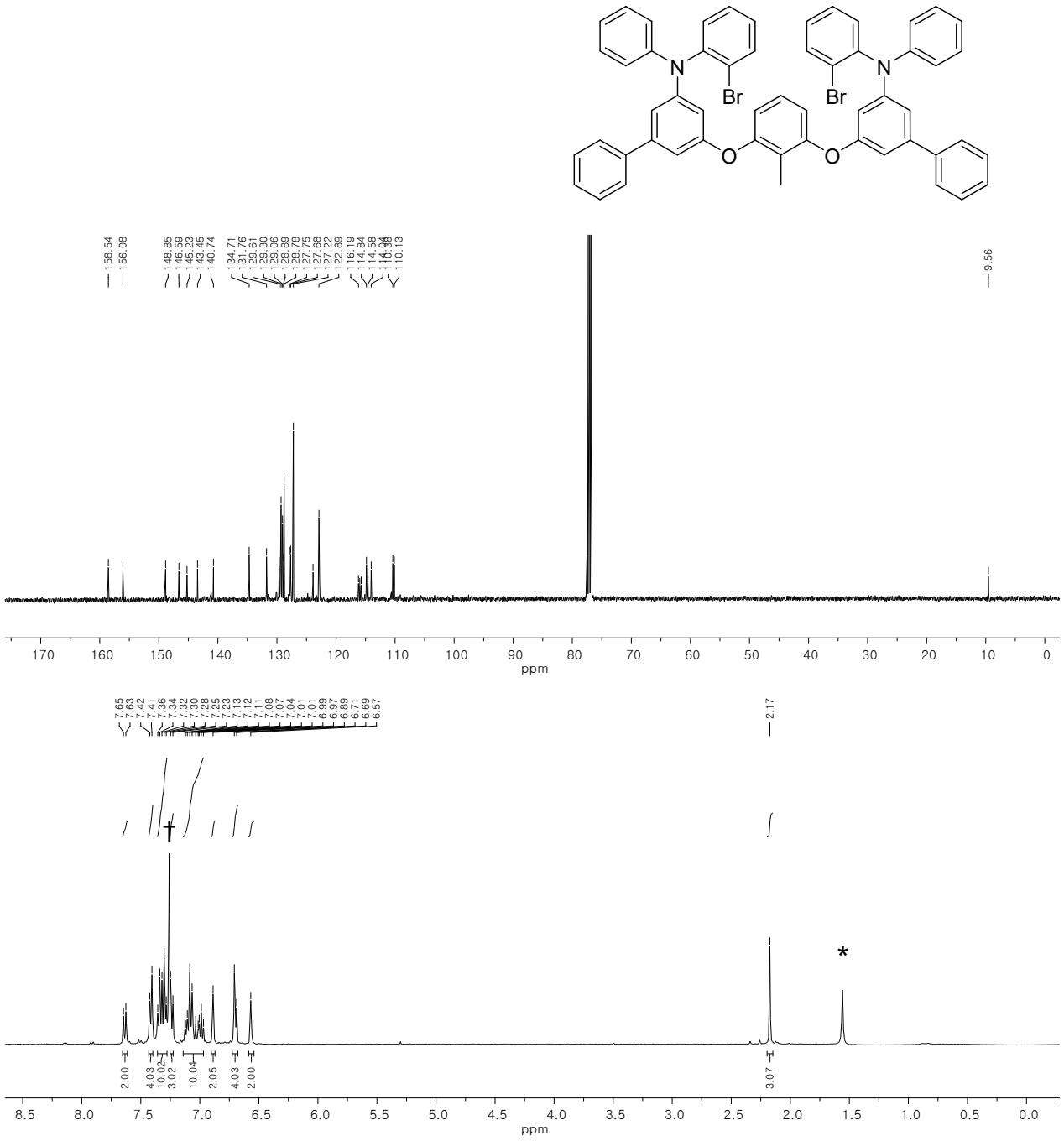

Fig. S12 ^{13}C (top) and ^{1}H (bottom) NMR spectra of **3e** (∗ and † from residual solvents).

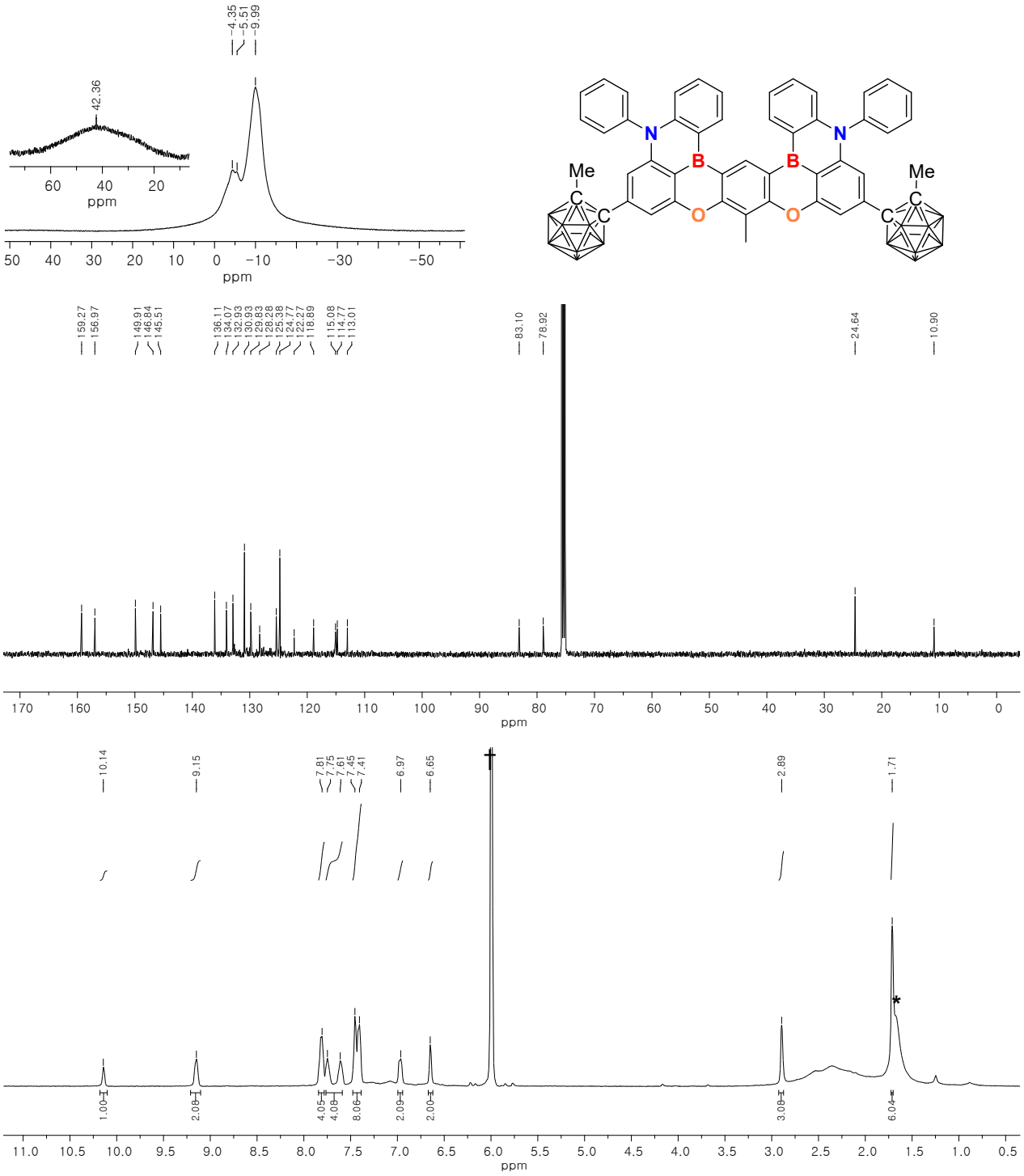

Fig. S13 ^{11}B (top), ^{13}C (middle), and ^{1}H (bottom) NMR spectra of **1** (∗ and † from residual solvents).

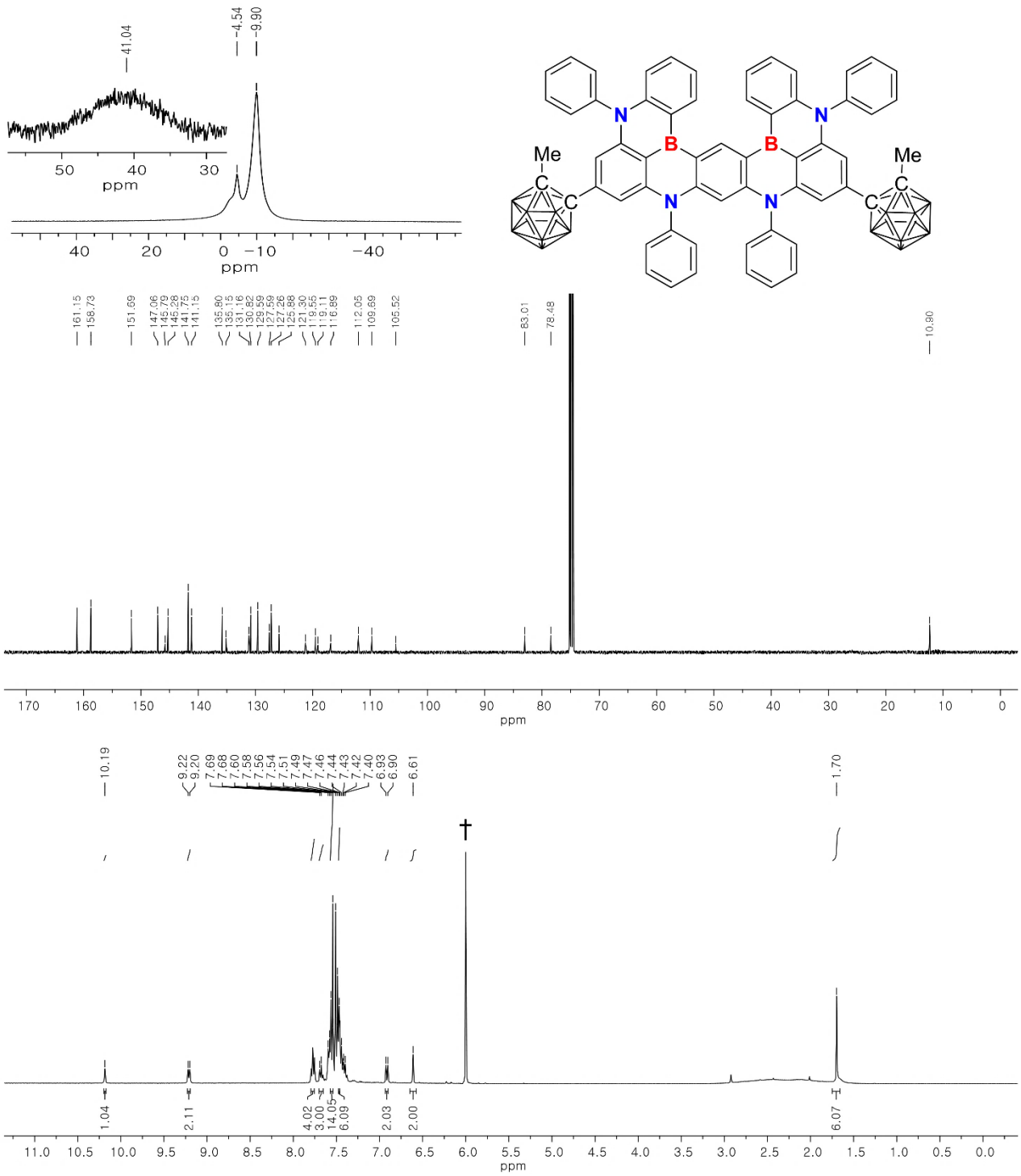

Fig. S14 ^{11}B (top), ^{13}C (middle), and ^{1}H (bottom) NMR spectra of **2** (∗ and † from residual solvents).

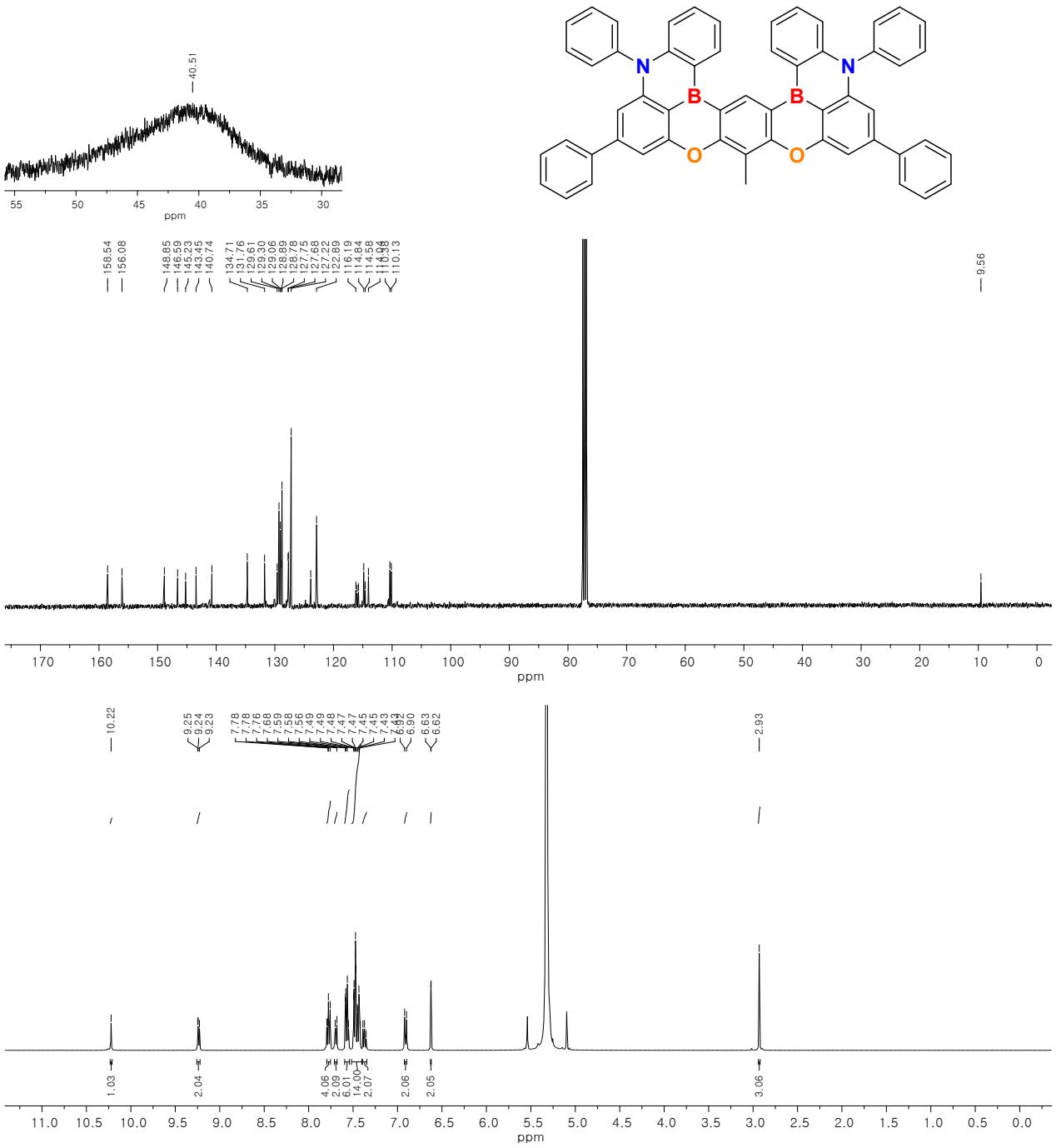

Fig. S15 ^{11}B (top), ^{13}C (middle), and ^{1}H (bottom) NMR spectra of **3** (∗ and † from residual solvents).

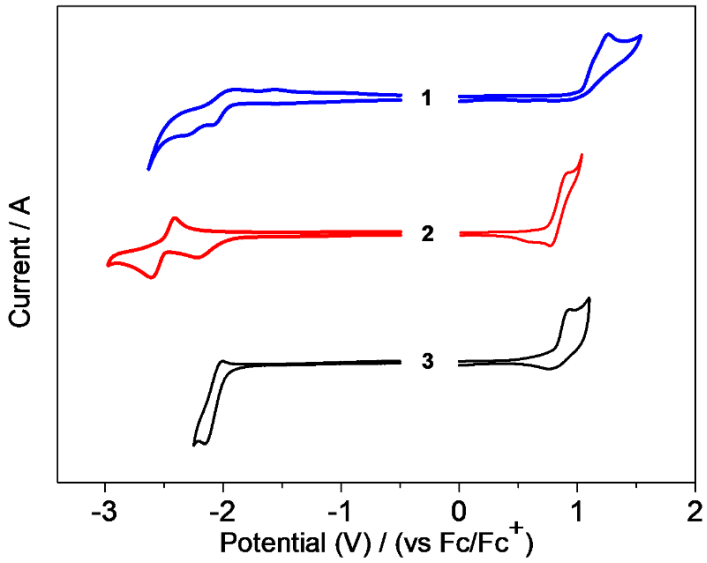

	E_g (eV)[a]	E_{ox} (V)[b]	E_{HOMO} (eV)[c]	E_{LUMO} (eV)[d]
1	2.72	1.03	−5.83	−3.11
2	2.51	0.75	−5.55	−3.04
3	2.74	0.80	−5.60	−2.86

[a] Optical bandgap from the absorption onset wavelength. [b] Onset potential (E_{onset}).

[c] From the E_{ox}. [d] From the E_g and E_{HOMO}.

Fig. S16 Cyclic voltammograms of **1**–**3** showing (right) oxidation in CH_2Cl_2 (1×10^{-3} M) and (left) reduction in DMF/THF (9:1, v/v, 1×10^{-3} M). Scan rate = 100 mV/s.

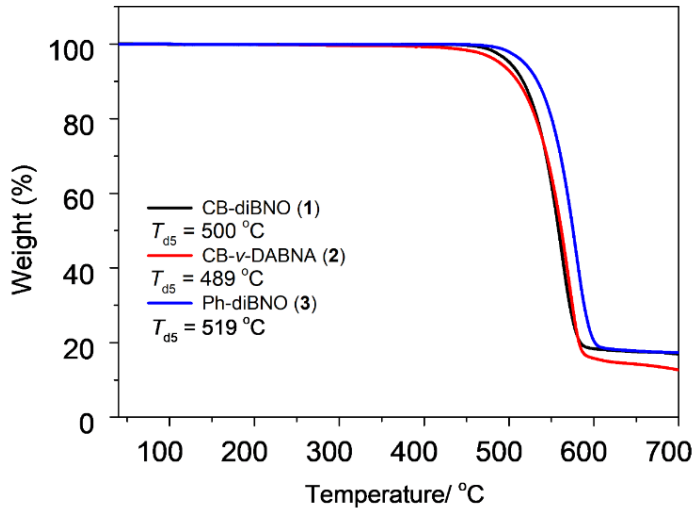

Fig. S17 TGA curves of **1**–**3**.

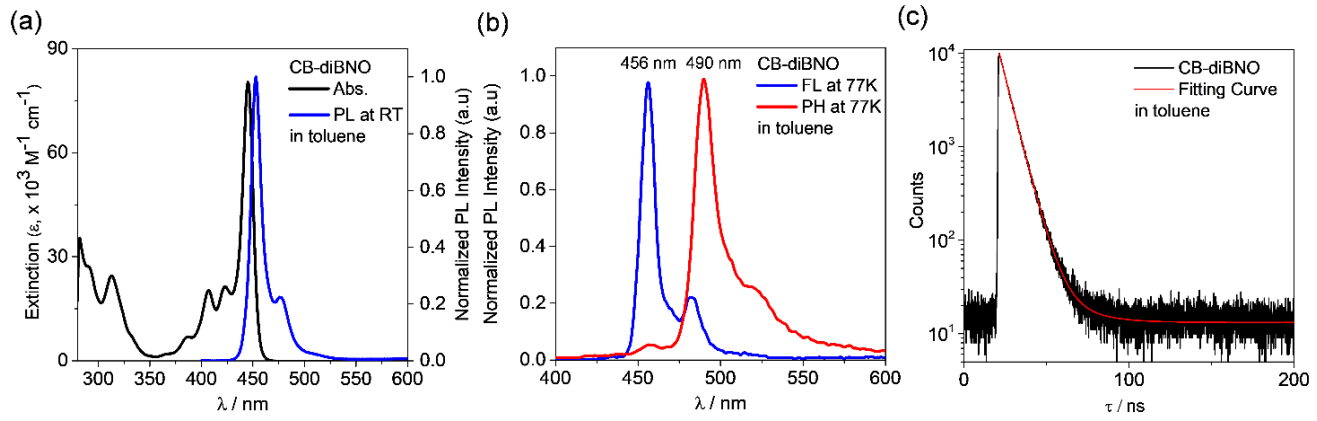

Fig. S18 (a) UV/Vis absorption and PL spectra at RT, (b) fluorescence and phosphorescence spectra at 77 K, and (c) transient PL decay of CB-diBNO (**1**) in toluene (1.0×10^{-5} M).

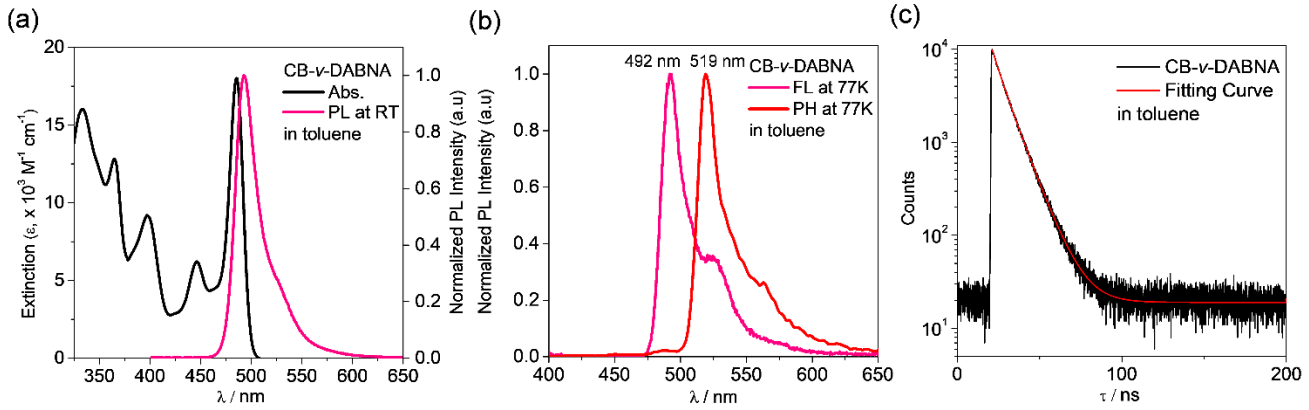

Fig. S19 (a) UV/Vis absorption and PL spectra at RT, (b) fluorescence and phosphorescence spectra at 77 K, and (c) transient PL decay of CB-*v*-DABNA (**2**) in toluene (1.0×10^{-5} M).

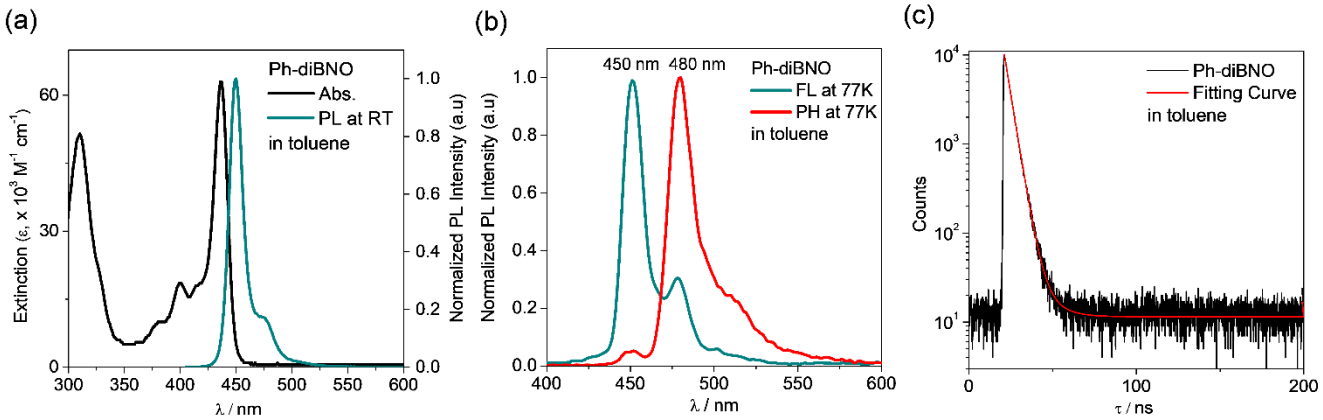

Fig. S20 (a) UV/Vis absorption and PL spectra at RT, (b) fluorescence and phosphorescence spectra at 77 K, and (c) transient PL decay of Ph-diBNO (**3**) in toluene (1.0×10^{-5} M).

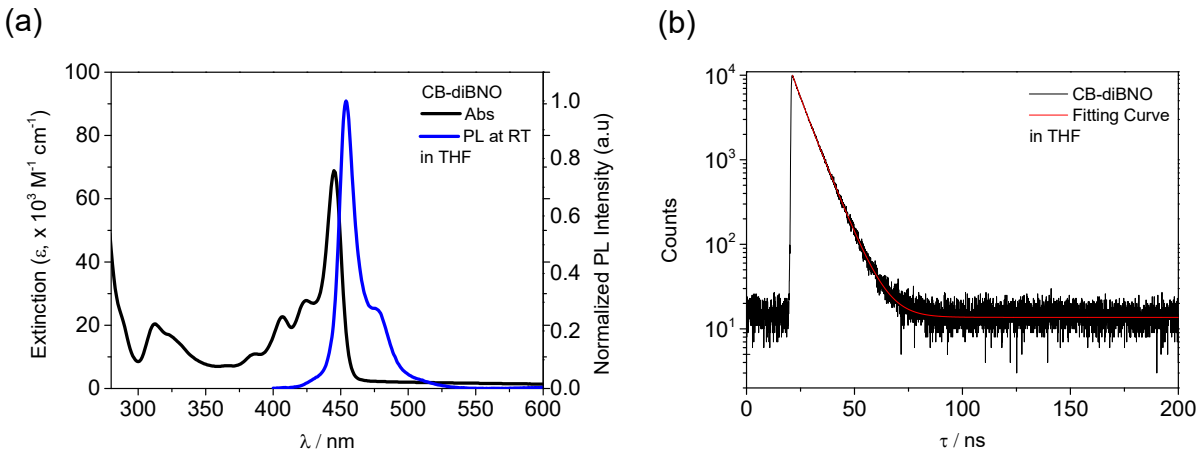

Fig. S21 (a) UV/Vis absorption and PL spectra at RT and (b) transient PL decay of CB-diBNO (**1**) in THF (1.0×10^{-5} M).

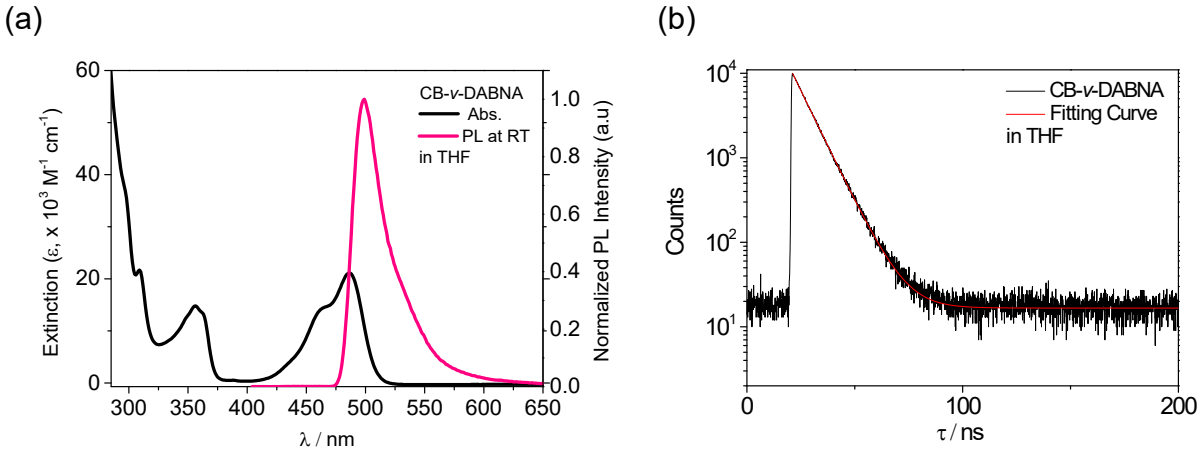

Fig. S22 (a) UV/Vis absorption and PL spectra at RT and (b) transient PL decay of CB-*v*-DABNA (**2**) in THF (1.0×10^{-5} M).

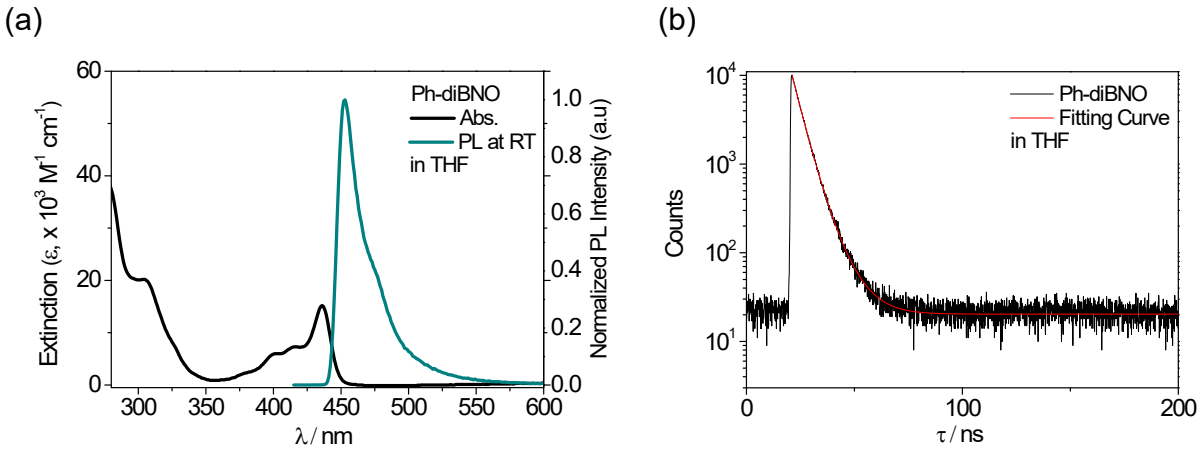

Fig. S23 (a) UV/Vis absorption and PL spectra at RT and (b) transient PL decay of Ph-diBNO (**3**) in THF (1.0×10^{-5} M).

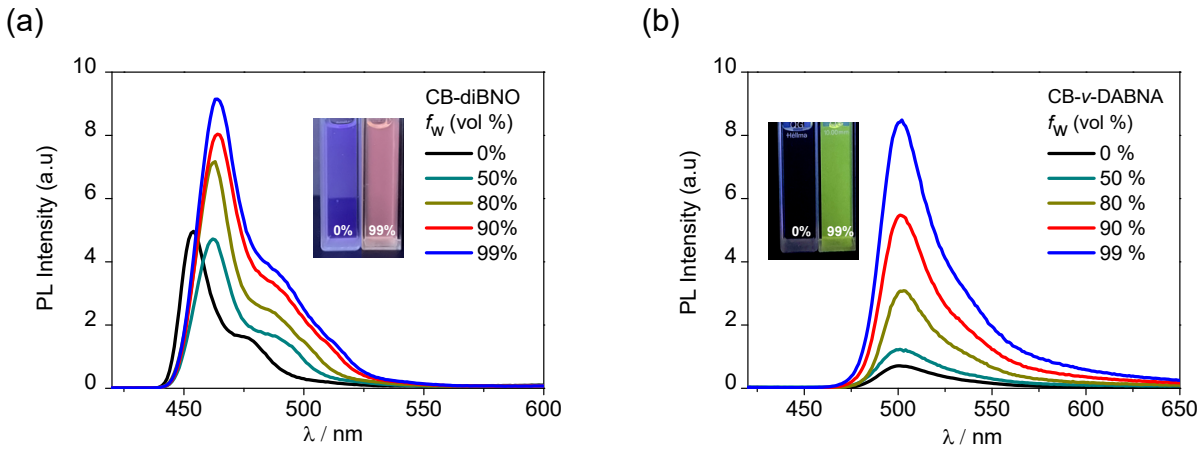

Fig. S24 PL spectra of (a) CB-diBNO (**1**) and (b) CB-*v*-DABNA (**2**) in THF/water mixtures (1.0×10^{-5} M) with various water fractions (f_w). Inset: Photos of **1** (left) and **2** (right) in THF/water mixtures (f_w = 0% and 99%) taken under 365 nm excitation.

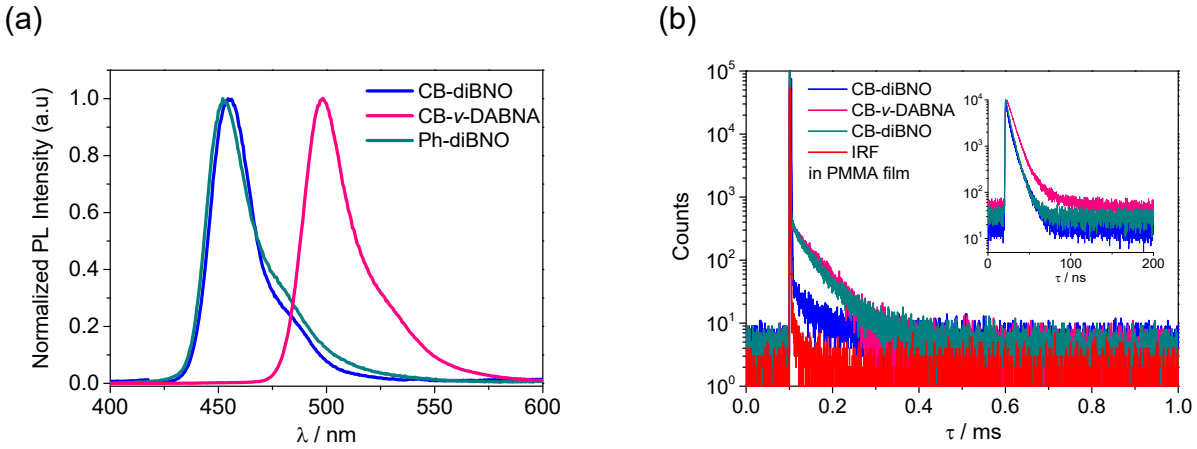

Fig. S25 (a) PL spectra and (b) transient PL decay curves of the PMMA films doped with 1 wt% of CB-diBNO (**1**), CB-*v*-DABNA (**2**), and Ph-diBNO (**3**). Inset: prompt PL decay.

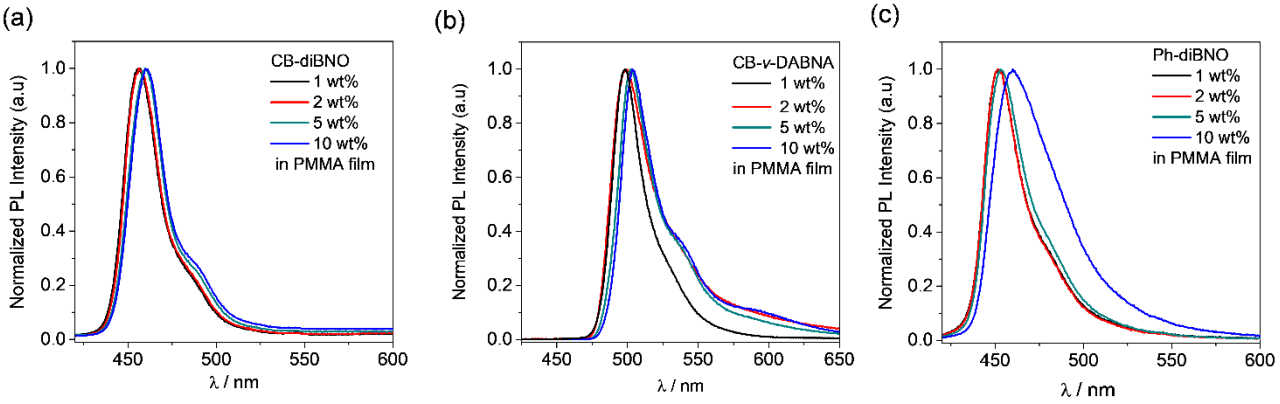

Fig. S26 PL spectra of the PMMA films doped with 1–10 wt% of (a) CB-diBNO (**1**), (b) CB-*v*-DABNA (**2**), and (c) Ph-diBNO (**3**).

Table S1 Photophysical data and rate constants of 1 wt% CB-diBNO (**1**), CB-*v*-DABNA (**2**), and BuDABNA (**3**) in PMMA.

compd	λ_{PL} (nm)	FWHM (nm)	Φ_{PL} (%)	Φ_p/Φ_d (%)[a]	τ_p (ns)/ τ_d (μs)[b]	ΔE_{ST} (eV)[c]	k_r (10^7 s^{-1})[d]	k_{ISC} (10^7 s^{-1})[d]	k_{RISC} (10^4 s^{-1})[d]
1	454	22	53	51/2	8.26/29.4	0.18	6.22	0.37	3.51
2	498	25	68	43/25	9.30/21.7	0.13	4.60	3.98	7.32
3	452	25	76	64/12	5.64/27.7	0.16	10.1	2.85	4.30

[a] PLQYs of prompt (Φ_p) and delayed (Φ_d) fluorescence ($\Phi_{PL} = \Phi_p + \Phi_d$). [b] Lifetimes of prompt (τ_p) and delayed (τ_d) PL decay components. [c] $\Delta E_{ST} = E_S - E_T$. [d] k_r, k_{ISC}, and k_{RISC} are the rate constants of fluorescence radiative decay, intersystem crossing, and reverse intersystem crossing (RISC), respectively.[15]

Table S2 Molecular orbital distributions (in %) of CB-diBNO (**1**), CB-*v*-DABNA (**2**), and Ph-diBNO (**3**) at their ground state (S_0) optimized geometries.

Compound	MO	Blue region	Red region	CB	others
1	HOMO	83.73	13.44	0.64	2.19
	LUMO	21.54	70.69	6.61	1.15
2	HOMO	84.82	11.56	0.74	2.88
	LUMO	22.11	69.31	7.45	1.14
3	HOMO	83.96	13.52	-	2.51
	LUMO	19.02	69.99	-	10.99

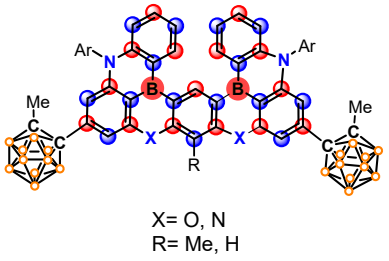

Blue: HOMO part
Red: LUMO part
CB: 2-Me-carborane

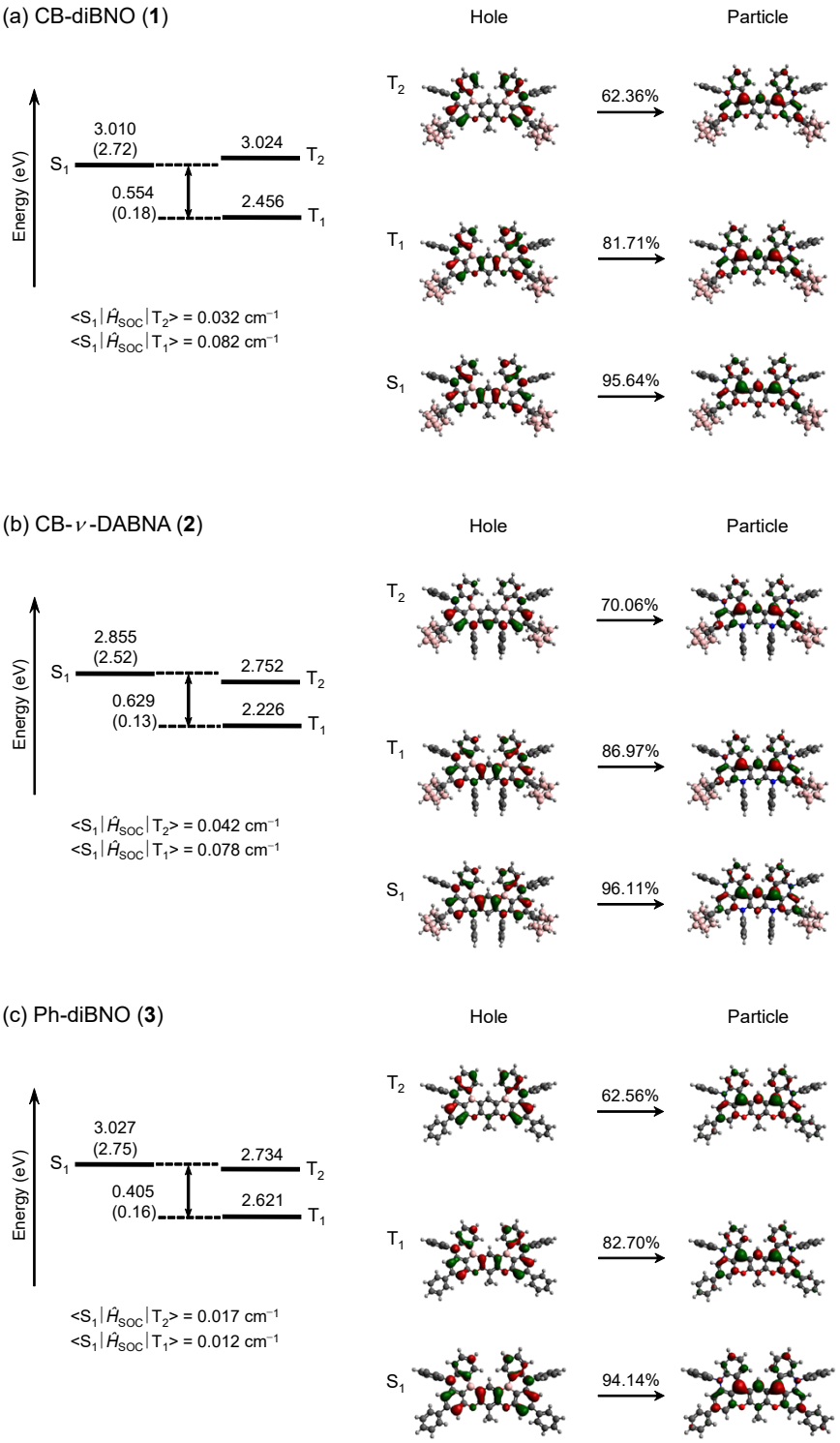

Fig. S27 Energy diagram for S_0 to S_1, T_1, and T_2 states, obtained in toluene medium, and natural transition orbitals (NTOs, isovalue = 0.03 e/Å^3) of (a) CB-diBNO (**1**), (b) CB-*ν*-DABNA (**2**), and Ph-diBNO (**3**) for the transitions from S_0 to S_1, T_1, and T_2 states. Along with the experimentally measured ΔE_{ST} values, corrected S_1 energies are presented in parentheses since TDDFT calculation is known to overestimate ΔE_{ST} for MR-TADF molecules due to an inaccurate estimation of the Coulomb interaction mainly for S_1 state.[16,17] Computationally obtained spin-orbit coupling matrix elements between the S_1 and T_n (n = 1 and 2) states at 298 K are provided.

Table S3 NTO contributions (in %) of CB-diBNO (**1**) and CB-*v*-DABNA (**2**) for the transitions from S_0 to S_1 and T_1 states.

State		Blue region	Red region	CB
S_1				
1	Hole	97.47	1.91	0.63
	Particle	91.93	0.61	7.46
2	Hole	96.72	2.55	0.72
	Particle	90.69	0.59	8.72
T_1				
1	Hole	97.45	1.91	0.64
	Particle	92.76	0.62	6.61
2	Hole	96.95	2.61	0.59
	Particle	91.97	0.74	7.45

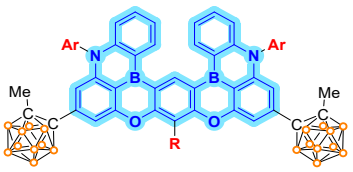

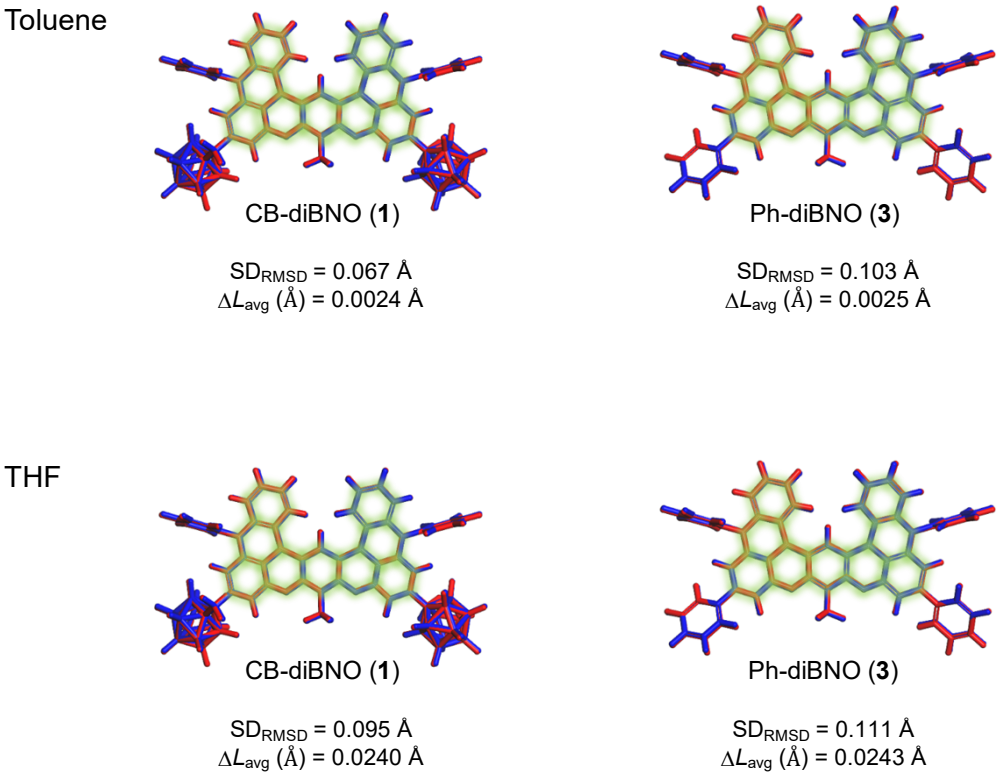

Fig. S28 Geometric overlap of the ground state (S_0, blue) and lowest singlet excited state (S_1, red) optimized structures of CB-diBNO (**1**) and Ph-diBNO (**3**) in toluene and THF. During the transition from S_1 to S_0 for these diboron MR-TADF compounds, the root-mean-square displacements (SD_{RMSD}) for the molecules and average changes in C–C bond lengths (ΔL_{avg}) for the structural deviation of highlighted MR-emitting core are provided.

Fig. S29 (a) Fluorescence spectra in THF at RT (red) and simulated emission spectra obtained from Franck–Condon analysis (black) for both compounds **1** (top) and **3** (bottom), where FC2 is the square of Franck-Condon factor. (b) Huang-Rhys (HR^k) factor and reorganization energy (λ_{ROE}^{k}) of each vibrational mode *k* contributing to the $S_1 \rightarrow S_0$ transition of **1** and **3**. (c) Vibrational normal modes, mode #8 and mode #3, mainly contributing to the spectral broadening of **1** and **3**, respectively.

Table S4 The vibrational modes contributing to the Franck-Condon spectral progression for CB-diBNO (**1**) in toluene. (FC2: the square of Franck-Condon factor). Three of the most intense peaks in each region were selected. The most intense peak in the main peak region is indicated in bold.

PL peak		Vibrational modes				
Wavelength (nm)[a]	FC^2	3	5	18	28	30
Main peak region						
451.92	**2.13×10^{-1}**	**0**[b]	**0**	**0**	**0**	**0**
452.38	1.26×10^{-1}	0	1	0	0	0
455.95	2.19×10^{-2}	0	0	0	1	0
Shoulder peak region						
456.40	2.38×10^{-3}	1	0	0	0	1
456.69	1.80×10^{-3}	1	1	0	1	0
457.80	1.22×10^{-3}	0	0	1	0	1

[a] The numerical values of computationally estimated wavelengths were corrected by increasing 24.31 nm to align with the peak position of the experimental PL spectrum. [b] The number *n* indicates the transition from the vibrational state $v = 0$ of S_1 state to the vibrational state $v = n$ of S_0 state.

Table S5 The vibrational modes contributing to the Franck-Condon spectral progression for Ph-diBNO (**3**) in toluene. (FC2: the square of Franck-Condon factor). Three of the most intense peaks in each region were selected. The most intense peak in the main peak region is indicated in bold.

PL peak		Vibrational normal modes		
Wavelength (nm)[a]	FC^2	3	6	8
Main peak region				
447.54	4.04×10^{-2}	0[b]	0	0
447.99	**4.74×10^{-2}**	**1**	**0**	**0**
448.44	3.00×10^{-2}	2	0	0
Shoulder peak region				
448.89	1.40×10^{-2}	1	1	0
448.90	1.36×10^{-2}	3	0	0
448.93	1.77×10^{-2}	1	0	1

[a] The numerical values of computationally estimated wavelengths were corrected by increasing 22.02 nm to align with the peak position of the experimental PL spectrum. [b] The number *n* indicates the transition from the vibrational state $v = 0$ of S_1 state to the vibrational state $v = n$ of S_0 state.

Table S6 The vibrational modes contributing to the Franck-Condon spectral progression for CB-diBNO (**1**) in THF. (FC2: the square of Franck-Condon factor). Three of the most intense peaks in each region were selected. The most intense peak in the main peak region is indicated in bold.

PL peak		Vibrational modes			
Wavelength (nm)[a]	FC^2	7	8	28	30
Main peak region					
452.28	3.72×10^{-2}	0[b]	0	0	0
452.75	$\mathbf{5.09\times10^{-2}}$	**1**	**0**	**0**	**0**
453.24	3.14×10^{-2}	1	1	0	1
Shoulder peak region					
456.73	5.16×10^{-3}	1	0	1	0
456.89	3.93×10^{-3}	1	0	0	1
456.24	3.77×10^{-3}	0	0	1	0

[a] The numerical values of computationally estimated wavelengths were corrected by increasing 20.22 nm to align with the peak position of the experimental PL spectrum. [b] The number *n* indicates the transition from the vibrational state $v = 0$ of S_1 state to the vibrational state $v = n$ of S_0 state.

Table S7 The vibrational modes contributing to the Franck-Condon spectral progression for Ph-diBNO (**3**) in THF. (FC2: the square of Franck-Condon factor). Three of the most intense peaks in each region were selected. The most intense peak in the main peak region is indicated in bold.

PL peak		Vibrational normal modes	
Wavelength (nm)[a]	FC^2	3	27
Main peak region			
450.42	3.06×10^{-2}	0[b]	0
450.89	$\mathbf{4.77\times10^{-2}}$	**1**	**0**
451.35	3.87×10^{-2}	2	0
Shoulder peak region			
454.79	2.72×10^{-3}	1	1
455.26	4.24×10^{-3}	3	0
455.74	3.43×10^{-3}	1	0

[a] The numerical values of computationally estimated wavelengths were corrected by increasing 20.31 nm to align with the peak position of the experimental PL spectrum. [b] The number *n* indicates the transition from the vibrational state $v = 0$ of S_1 state to the vibrational state $v = n$ of S_0 state.

Table S8 Details of parameters employed for the simulation of PL spectrum in Toluene using MOMAP software.

parameter	value	parameter	value
FreqScale	1.0	Steps	0.0000001
Maxvib	10	FWHM	500 cm^{-1} (THF: 600 cm^{-1})
promode	24	blocksize	1000
FC_eps_abs	0.012 (THF: 0.04)	testpoints	1000
FC_eps_emi	0.012 (THF: 0.04)	reduce_eps	0.001
FC_eps_ic	0.012 (THF: 0.04)		

(a)

Ph-diBNO

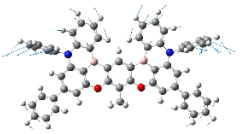

3 (20.4 cm^{-1})
λ_{ROE}^{mode} = 26.3
HR^{3} = 1.289

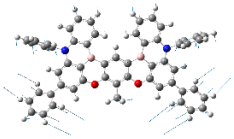

6 (40.65 cm^{-1})
λ_{ROE}^{mode} = 12.28
HR^{6} = 0.302

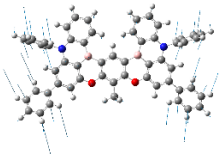

8 (42.48 cm^{-1})
λ_{ROE}^{mode} = 15.91
HR^{8} = 0.375

CB-diBNO

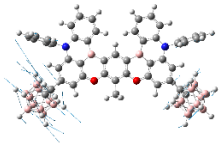

3 (12.07 cm^{-1})
λ_{ROE}^{mode} = 1.66
HR^{3} = 0.137

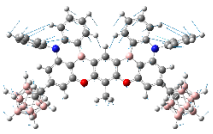

5 (19.94 cm^{-1})
λ_{ROE}^{mode} = 13.53
HR^{5} = 0.679

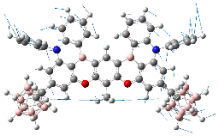

18 (72.65 cm^{-1})
λ_{ROE}^{mode} = 5.17
HR^{18} = 0.071

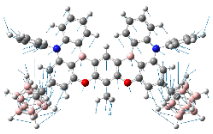

28 (176.07 cm^{-1})
λ_{ROE}^{mode} = 18.25
HR^{28} = 0.104

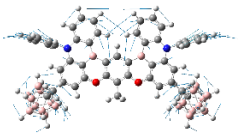

30 (183.36 cm^{-1})
λ_{ROE}^{mode} = 14.78
HR^{30} = 0.081

(b)

Ph-diBNO

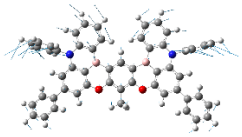

3 (21.02cm^{-1})
λ_{ROE}^{mode} = 34.86
HR^{3} = 1.658

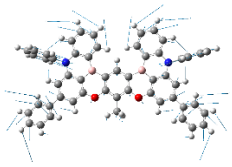

27 (195.35 cm^{-1})
λ_{ROE}^{mode} = 17.25
HR^{27} = 0.088

CB-diBNO

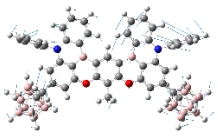

7 (21.35 cm^{-1})
λ_{ROE}^{mode} = 20.87
HR^{7} = 0.978

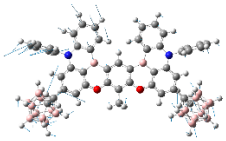

8 (21.69 cm^{-1})
λ_{ROE}^{mode} = 8.66
HR^{8} = 0.399

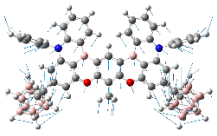

28 (176.01 cm^{-1})
λ_{ROE}^{mode} = 17.98
HR^{28} = 0.102

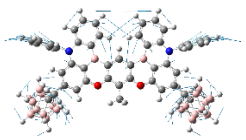

30 (183.38 cm^{-1})
λ_{ROE}^{mode} = 14.24
HR^{30} = 0.078

Fig. S30 Selected vibrational modes (see **Table S4**–**S7**) and their vibrational frequencies for the S_1–S_0 transition of CB-diBNO (**1**) and Ph-diBNO (**3**) (a) in toluene and (b) in THF. Their reorganization energy (λ_{ROE}^{mode}, cm^{-1}) and dimensionless Huang-Rhys factor (HR^{mode}) of each vibrational mode are provided.

Table S9 Selected reports of MR-TADF compounds with narrow FWHM (≤ 15 nm).

compound	λ_{PL} (nm)	FWHM (nm)	medium	ref
CB-diBNO (**1**)	453	11	Toluene	This work
v-DABNA	468	14	Toluene	[18]
BOBO-Z	441	15	Toluene	[19]
m-*v*-DABNA	464	14	Toluene	[20]
4F-*v*-DABNA	457	14	Toluene	[20]
4F-m-*v*-DABNA	455	14	Toluene	[20]
t-Bu-*v*-DABNA	467	14	Toluene	[21]
o-Tol-*v*-DABNA-Me	466	14	Toluene	[22]
NO-DBMR	458	14	Toluene	[23]
Cz-DBMR	480	14	Toluene	[23]
V-DABNA	483	14	Toluene	[24]
V-DABNA-F	467	13	Toluene	[24]
V-DABNA-Mes	486	13	Toluene	[25]
CzB4	470/483	11/14	3-Methylpentane/ 0.1wt%-PS	[26]
CzB6	475/488	14/12	3-Methylpentane/ 0.1wt%-PS	[26]
CzB8	485/491	20/12	3-Methylpentane/ 0.1wt%-PS	[26]
CzB4-oPh	467/478	9/16	3-Methylpentane/ 0.1wt%-PS	[26]
TB-PB	473	12	Toluene	[27]

References

1. S. Nakatsuka, H. Gotoh, K. Kinoshita, N. Yasuda and T. Hatakeyama, *Angew. Chem. Int. Ed.*, 2017, **56**, 5087-5090.
2. S. Hirata and M. Head-Gordon, *Chem. Phys. Lett.* 1999, **314**, 291-299.
3. C. Adamo and V. Barone, *J. Chem. Phys.* 1999, **110**, 6158.
4. F. Weigend and R. Ahlrichs, *Phys. Chem. Chem. Phys.* 2005, **7**, 3297.
5. M. J. Frisch, G. W. Trucks, H. B. Schlegel, G. E. Scuseria, M. A. Robb, J. R. Cheeseman, G. Scalmani, V. Barone, G. A. Petersson, H. Nakatsuji, X. Li, M. Caricato, A. V. Marenich, J. Bloino, B. G. Janesko, R. Gomperts, B.; Mennucci, H. P. Hratchian, J. V. Ortiz, A. F. Izmaylov, J. L. Sonnenberg, D. Williams-Young, F.; Ding, F. Lipparini, F. Egidi, J. Goings, B. Peng, A.Petrone, T. Henderson, D. Ranasinghe, V. G. Zakrzewski, J. Gao, N. Rega, G. Zheng, W. Liang, M. Hada, M. Ehara, K. Toyota, R. Fukuda, J. Hasegawa, M. Ishida, T. Nakajima, Y. Honda, O. Kitao, H. Nakai, T. Vreven, K. Throssell, J. A. Montgomery, J. E. Jr.; Peralta, F. Ogliaro, M. J. Bearpark, J. J Heyd, E. N. Brothers, K. N. Kudin, V. N. Staroverov, T. A. Keith, R. Kobayashi, J. Normand, K. Raghavachari, A. P. Rendell, J. C. Burant, S. S. Iyengar, J. Tomasi, M. Cossi, J. M. Millam, M. Klene, C. Adamo, R. Cammi, J. W. Ochterski, R. L. Martin, K. Morokuma, O. Farkas, J. B. Foresman and D. J. Fox, Gaussian 16, Revision C.01, Gaussian, Inc., Wallingford CT, 2019.
6. J. Tomasi, B. Mennucci and R. Cammi, *Chem. Rev.* 2005, **105**, 2999-3093
7. R. L. Martin, *J. Chem. Phys.* 2003, **118**, 4775
8. T. Lu, F. Chen, *J. Comput. Chem*. 2012, **33**, 580
9. S. I. Gorelsky and A. B. P. Lever, *J. Organomet. Chem.* 2001, **635**, 187.
10. B. de Souza, G. Farias, F. Neese and R. Izsak, *J. Chem. Theory Comput.* 2019, **15**, 1896
11. (a) F. Neese, *WIREs Comput. Mol. Sci.* **2011**, *2*, 73-78. (b) F. Neese, *WIREs Comput. Mol. Sci.* 2018, **8**, e1327.
12. W. Humphrey, A. Dalke and K. Schulten, *J. Molec. Graphics*, 1996, **14**, 33-38.
13. Y. Niu, W. Li, Q. Peng, H. Geng, Y. Yi, L. Wang, G. Nan, D. Wang and Z. Shuai, *Mol. Phys.* 2018, **116**, 1078-1090.
14. a) Z. Shuai, *Chin. J. Chem.* 2020, **38**, 1223-1232; b) Z. Shuai and Q. Peng, *Phys. Rep.* 2014, **537**, 123-156.
15. R. Furue, K. Matsuo, Y. Ashikari, H. Ooka, N. Amanokura and T. Yasuda, *Adv. Optical Mater.* 2018, **6**, 1701147.
16. K. Shizu, H. Kaji, *Commun. Chem.* **2022**, *5*, 53.
17. A. Pershin, D. Hall, V. Lemaur, J. C. Sancho-Garcia, L. Muccioli, E. Zysman-Colman, D. Beljonne, Y. Olivier, *Nat. Commun.* **2019**, *10*, 597.
18. Y. Kondo, K. Yoshiura, S. Kitera, H. Nishi, S. Oda, H. Gotoh, Y. Sasada, M. Yanai and T. Hatakeyama, *Nat. Photonics*, 2019, **13**, 678.
19. I. S. Park, M. Yang, H. Shibata, N. Amanokura and T. Yasuda, *Adv. Mater*. 2022, **34**, 2107951.
20. K. R. Naveen, H. Lee, R. Braveenth, K. J. Yang, S. J. Hwang and J. H. Kwon, *Chem. Eng. J*., 2022, **432**, 134381.
21. K. R. Naveen, H. Lee, R. Braveenth, D. Karthik, K. J. Yang, S. J. Hwang and J. H. Kwon, *Adv. Funct. Mater*., 2022, **32**, 2110356.
22. H. S. Kim, H. J. Cheon, D. G. Lee, W. C. Lee, J. H. Kim, Y. H. Kim and S. H. Yoo, *Sci. Adv*., 2023, **9**,

eadf1388.

23. K. R. Naveen, J. H. Oh, H. S. Lee and J. H. Kwon, *Angew. Chem. Int. Ed*. 2023, **62**, e202306768.

24. S. Oda, B. Kawakami, M. Horiuchi, Y. Yamasaki, R. Kawasumi and T. Hatakeyama, *Adv. Sci.*, 2023, **10**, 2205070.

25. S. Oda, B. Kawakami, Y. Yamasaki, R. Matsumoto, M. Yoshioka, D. Fukushima, S. Nakatsuka and T. Hatakeyama, *J. Am. Chem. Soc.*, **2022**, 144, 106–112.

26. Y. Sano, T. Shintani, M. Hayakawa, S. Oda, M. Kondo, T. Matsushita and T. Hatakeyama, *J. Am. Chem. Soc.*, 2023, **145**, 11504–11511.

27. W. Yuan, Q. Jin, M. Du, L. Duan and Y. Zhang, *Adv. Mater.*, 2024, **36**, 2410096.